SCIENCE CHINA
Information Sciences

June 2020, Vol. 63 160404:1–160404:24
https://doi.org/10.1007/s11432-020-2883-0

• REVIEW •
Special Focus on Photonics in AI

Automatic mode-locking fiber lasers: progress and perspectives

Guoqing PU, Li ZHANG, Weisheng HU & Lilin YI*

State Key Lab of Advanced Communication Systems and Networks, Shanghai Institute for Advanced Communication and Data Science, Shanghai Jiao Tong University, Shanghai 200240*, China*

Received 6 February 2020/Revised 18 March 2020/Accepted 20 April 2020/Published online 13 May 2020

Abstract Polarization control in nonlinear polarization rotation based mode-locked fiber lasers is a long-term challenge. Suffering from the polarization drifts induced by environmental disturbances, nonlinear polarization rotation based mode-locked fiber lasers is difficult in continuously operating under the desired pulsation regime thereby substantially hindering their utilizations. The appearance of automatic mode-locking techniques brings the light in addressing this challenge. Combining with various algorithms and electrical polarization control, automatic mode-locking techniques resolve the dilemma of nonlinear polarization rotation based mode-locked fiber lasers. We review the research progress of automatic mode-locking techniques in detail. Furthermore, we comment on the perspectives and potential applications of automatic mode-locking techniques.

Keywords nonlinear polarization rotation, ultrashort pulses, automatic mode-locking, electrical polarization control, optimization algorithms, machine learning, time stretch

Citation Pu G Q, Zhang L, Hu W S, et al. Automatic mode-locking fiber lasers: progress and perspectives. Sci China Inf Sci, 2020, 63(6): 160404, https://doi.org/10.1007/s11432-020-2883-0

1 Introduction

Ultrashort optical pulses have extensive utilizations ranging from optical frequency measurements [1–4] to high-resolution atomic clocks [5, 6], signal processing [7, 8], ranging metrology [9, 10], and astronomy [11, 12]. As the primary means of generating ultrashort pulses, mode-locking techniques have experienced explosive development over the last several decades and remain one of the most active research areas in photonics [13]. Mode-locking is a resonant phenomenon, which represents locking the phases of numerous longitudinal modes inside the laser cavity thereby producing a pulsed radiation [14, 15]. In terms of the realization methods, mode-locking techniques can be sorted into three categories including actively mode-locking [15], passively mode-locking [13] and hybrid mode-locking [16]. Nonlinear polarization rotation (NPR) additive pulse mode-locking relying on polarization control and Kerr nonlinearities [13, 15] is preferred by researchers to realize passively mode-locked fiber lasers (MLFLs) owing to its simple structure and superior performance [17–20]. The simplified principle of this method is to use the Kerr nonlinearity in the fiber, the intensity-dependent nonlinear phase shift causes the change in the polarization state as a function of the light intensity [13, 15]. Therefore, an effective fast artificial saturable absorber can be observed by aligning the output polarizer in such a way that the high intensity experiences a lower loss [13]. Moreover, through flexible polarization control, NPR-based MLFLs can produce various pulsation regimes including the most common fundamental mode-locking (FML) regime, harmonic mode-locking (HML)

* Corresponding author (email: lilinyi@sjtu.edu.cn)

regimes [19–21] with high repetition rate, Q-switching (QS) regimes [22–24] with high pulse energy, and Q-switched mode-locking (QML) regimes [24,25] as well. However, manual polarization control is difficult to initially locate onto desired regimes especially rare regimes (i.e., excluding the FML regime) in NPR-based MLFLs owing to the small polarization solution space. In addition, inherent various transient instabilities of MLFLs [26] like the multi-pulsing instabilities [27–29] and Q-switched instabilities [30] further reduce the stability of NPR-based MLFLs. It is even harder to maintain NPR-based MLFLs (i.e., a resonant cavity with strong nonlinearities) operating under the desired regime through manual polarization control for a long time because of the polarization drifts induced by continuous environmental disturbances (e.g., thermal instability and mechanical vibration) [31–38]. However, long-term stability of NPR-based MLFLs is indeed desired in both academic and industrial applications because the QS instabilities during the detachments (i.e., the laser loses the desired pulsation regime) may cause irreversible damage to the sequent devices after lasers [39, 40].

To address the dilemma of NPR-based MLFLs, self-starting MLFLs [41–44], polarization maintaining fiber based MLFLs [44–48] and photonic crystal fiber based MLFLs [48–50] are demonstrated to improve the utility and stability. These techniques indeed gain certain effects but they do not completely resolve the dilemma of NPR-based MLFLs because the polarization drift induced by environmental disturbances is continuous [31–38]. Even the polarization drift in a short time is negligible for these MLFLs with stabilization mechanism like polarization maintaining fiber based MLFLs, long-term exposure to environmental disturbances will ultimately produce a large polarization drift very likely causing detachments [31]. Till then, recalibration and realignment of the lasers are necessary. Therefore, automatic mode-locking (AML) techniques, as a new research area in ultrafast lasers [17], underwent a tremendous growth in the last decade since the emergence. Different from the traditional stabilization techniques, AML techniques try to address the dilemma adaptively using various algorithms and electrical control on some parameters inside the cavity (e.g., electrical polarization control). AML starts from the characterization for an NPR-based MLFL (i.e., establishing a mapping between polarization states and system parameters including pulse duration, central wavelength and average output power), which assists the laser to fast locate the desired operation regime [51]. Then, the feedback scheme is introduced to AML thereby spawning many AML lasers achieved by the inefficient traversal algorithm [51–58] and some of these AML lasers still require manual auxiliary polarization control inside the laser cavity [51, 52]. Furthermore, smart lasers, intelligent lasers, self-tuning lasers using optimization algorithms [59–67], machine learning [68–71] and even deep learning [72] are proposed to improve the performance AML lasers. Concretely, an AML laser with superior performance requires no manual auxiliary polarization control inside the cavity. The laser should also have excellent time-consuming performance including the initial lock time (i.e., the time consumption from noise to the desired pulsation regime) and the recovery time (i.e., the time consumption of recovering from detachments). In addition, the laser should be able to automatically lock onto various regimes for different applications. We believe that the emergence of AML techniques will completely resolve the dilemma of NPR-based MLFLs thereby further broadening the utilizations of NPR-based MLFLs.

In this study, we review the research progress of AML techniques in detail. From Section 2 to Section 4, we respectively review the AML techniques enabled by the traversal algorithm, optimization algorithms and machine learning. Then in Section 5, we discuss the perspectives and potential applications of AML lasers and finally we conclude in Section 6.

2 AML enabled by the traversal algorithm

In the early stage of AML techniques, the traversal algorithm is the most frequently used algorithm. The traversal algorithm for AML techniques is usually consisted of a traversal process, which goes through the whole controllable parameter space like the polarization Poincaré sphere to meet the discrimination criteria for desired pulsation regimes. The common discrimination criteria include pulsing counting [52, 54, 56, 57] and detection of some special parameters [51, 53, 55, 58]. Although the traversal

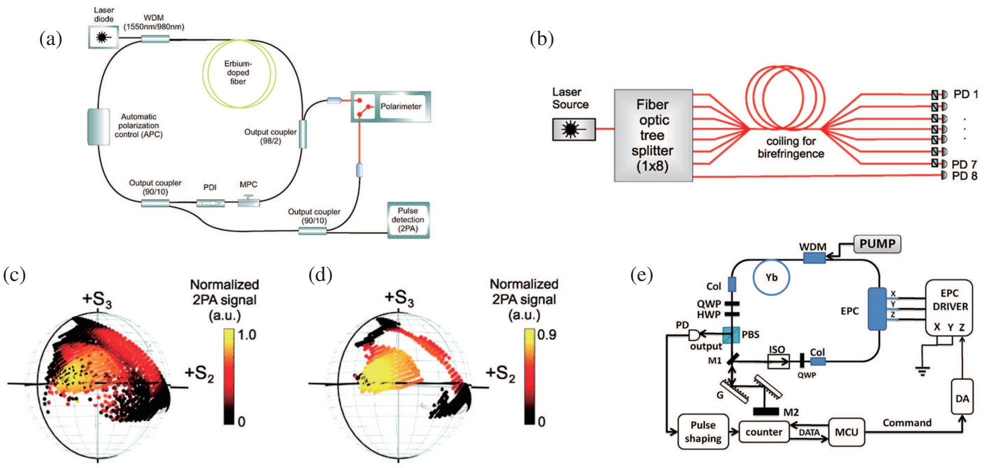

Figure 1 (Color online) (a) The experimental setup of automated characterization and alignment of an NPR based MLFL in [51]; (b) the design of the DOAP; (c) the scanning result of the pulsation regimes area on the Poincaré sphere; (d) the scanning result of the mode-locking regime area after numerical filtering. Reprinted with permission from [51] @Copyright 2010 Springer Nature. (e) The experimental setup of the electronic control of NPR based Yb-doped fiber MLFL in [52]. Reprinted with permission from [52] @Copyright 2012 Optical Society of America.

algorithm based AML lasers generally has non-ideal time-consuming performance owing to the inefficient search on the tremendous parameter space (may be multi-dimensional), these AML lasers are able to produce various regimes including the FML regime [51–58], HML regimes [57] and even noise-like pulses (NLPs) [58]. In addition, some of them are built in real-time implementations [52, 54, 56], where micro control unit (MCU) or field programmable gate array (FPGA) are used as the computation center and circuits like analog-to-digital converters (ADCs) are used to obtain feedback data. Different from the off-line implementations (large equipment is used for data acquisition and a computer is usually used as the computation center), AML lasers built in real-time implementations have enormous advantages over time-consuming performance.

The pioneer work in AML techniques was demonstrated back in 2010 [51]. Hellwig et al. successfully characterized an NPR-based erbium-doped MLFL using a computer-controlled automatic polarization controller (APC) based on piezoelectric squeezers and a home-made high-speed all-fiber division-of-amplitude polarimeter (DOAP). The entire experimental setup is demonstrated in Figure 1(a). The laser is fully characterized through automatic polarization scanning governed by the APC. The characterization of the laser means establishment of a mapping between polarization states and system parameters including pulse duration, central wavelength and average output power. The design of the DOAP is shown in Figure 1(b). The basic idea of the DOAP is to project the incident light into different polarization directions using multiple polarizers and then the polarization state of the incident light can be obtained from the power distribution on different polarization directions. In the DOAP, one fiber and a photodiode (PD 8) are utilized to acquire the reference power for normalization while the other seven fibers are randomly bent to introduce different values of birefringence in each of them [51]. It should be noted that the pulsation regimes are judged through measuring two-photon absorption (2PA) since only the high peak power of an ultrashort pulse will lead to strong 2PA. The automatic polarization scanning result on the Poincaré sphere is shown in Figure 1(c) and the polarization area corresponding to pulsation regimes has strong 2PA signal values. However, the pulsation regimes also contain QS and hybrid regimes (i.e., QML regimes [24, 25]). Through applying a numerical filter on the scanning result, the polarization area corresponding to mode-locking regime is obtained as shown in Figure 1(d). This study could help the NPR-based MLFLs fast locate on the mode-locking regime with excellent parameters. However, when the established mapping is not updated for a long time, it could fail to locate on the mode-locking regime. Although the authors performed a five-day test in the research, the time-variant cavity state (i.e., birefringence) is still a non-negligible challenge.

Shen et al. [52] realized AML in a NPR-based MLFL with a piece of Yb-doped fiber as the gain media.

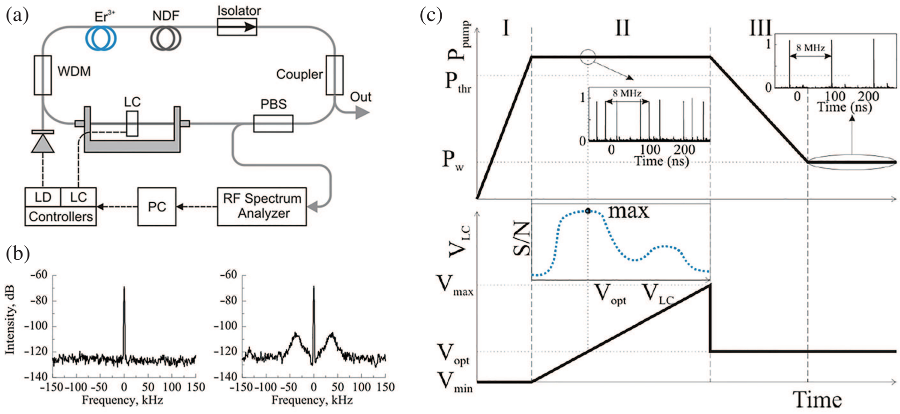

Figure 2 (Color online) (a) The experimental setup in [53]; (b) RF inter-mode beat spectrum of the most stable (left) and less stable (right) FML regime at around 8 MHz; (c) time diagram of the programmatically mode lock starting: pump power (P), the LC control voltage (V), relation between the magnitude of the peak of the RF inter-mode beat spectrum and the LC control voltage (dashed line). Reprinted with permission from [53] @Copyright 2013 Optical Society of America.

The experimental setup is shown in Figure 1(e). An electronic polarization controller (EPC), which has three integrated fiber squeezers with different orientations, is used to tune the polarization state inside the cavity via changing the strains on the fiber. The discrimination of mode-locking regime is based on pulse counting, which is achieved through an electrical pulse-shaping module and a counter module. The MCU is in charge of discriminating the current state based on the pulse counting result and controlling the EPC through a digital-to-analog converter (DAC) and an amplifier simultaneously. Notably, only one channel of the EPC is used in this experiment for simplicity. The basic operation logic behind the system is when the MCU discriminates the current state to be the mode-locking regime, the EPC tuning stops. Otherwise, the MCU continuously controlling the EPC to tune the polarization state inside the cavity using a traversal algorithm till mode-locking regime is searched. This research certainly has an unparalleled impact in the development of AML techniques since it firstly introduces feedback scheme into AML domain. However, the laser demonstrated in this research is more similar to a semi-AML laser. Because manual polarization control through quarter wave plates (QWPs) and half wave plate (HWP) inside the cavity is still needed when the mode-locking regime is not found after going through the EPC voltage range. It indeed puts a limitation on the wide applications of this laser. Sequentially, the same group further presented a method for stabilizing the repetition rate of an erbium-doped MLFL using the EPC. Under a repetition rate of 74.6 MHz, the standard deviation and the repetition rate linewidth were respectively 1.4 MHz and 1.7 MHz [73].

Radnatarov et al. [53] performed AML technique in a normal net dispersion cavity with a fundamental repetition rate of 8 MHz using a liquid-crystal (LC) variable retarder to electrically control the polarization state inside the cavity as shown in Figure 2(a). A phase delay of 0 to 0.6λ can be introduced by applying a control voltage not exceeding 4 V to the LC. They found that the maximum magnitude of the radio-frequency (RF) peak corresponds to the most stable FML regime in the absence of any side features in the RF inter-mode beat spectrum as shown in the left of Figure 2(b). However, as the magnitude slid off the maximum (owing to changing birefringence in the LC), the FML regime stability worsens and additional satellite peaks could emerge beside the main one in the RF beat spectrum as indicated in the right of Figure 2(b). Hence, through analyzing the RF spectrum, the stable FML regime can be discriminated. The algorithm is illustrated in Figure 2(c). The starting phase (I) of the algorithm corresponds to ramping up the pump output power until the laser enters into the unstable FML regime as shown in the upper part of Figure 2(c). $P_{\rm thr}$ is the threshold pump power of the mode-locking. After that, during phase II of the algorithm, the computer sweeps the voltage range applied to the LC so as to find the optimal value $V_{\rm opt}$ as shown in the lower part of Figure 2(c). The inset (dashed line) of Figure 2(c) demonstrates the variation of the magnitude of the peak of the RF inter-mode beat spectrum when the voltage applied to the LC is swept. Finally, in the subsequent phase (III) of the algorithm, the

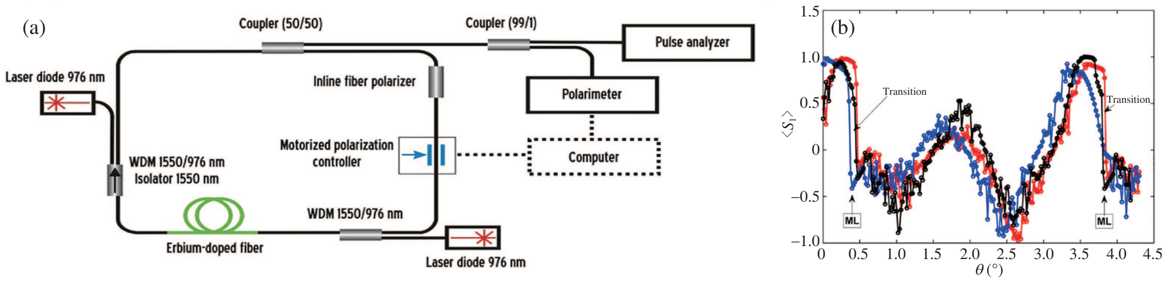

Figure 3 (Color online) (a) The experimental setup in [55]; (b) the averaged first Stokes parameter acquired when the steady FML regime is reached under unperturbed case (red), perturbation before Erbium-doped fiber (blue) and perturbation after Erbium-doped fiber (black). Reprinted with permission from [55] @Copyright 2015 Optical Society of America.

voltage applied to the LC is set to $V_{\rm opt}$ and the pump power is gradually reduced until the multi-pulse mode-locking regime transitioned to the FML regime. This study is a great progress in automatic MLFL since manual polarization control is not needed in the cavity for the first time, therefore, it provides endless possibilities for the applications of automatic MLFL in the future.

Then, Li et al. [54] realized an automatic MLFL with a repetition rate of 6.238 MHz using two EPCs. Analogous to the previous study [52], an MCU runs a traversal algorithm to search the mode-locking regime and the discrimination of the mode-locking regime is based on the pulse counting after pulse shaping (shaping to a square with a lower repetition rate). According to the experiments, the laser can automatically get into the mode-locking regime within 90 s after turning the system on (i.e., the initial lock time). This is a good study but the performance can still be improved. Different applications require different pulsation regimes. The automatic system can only search the FML regime and may be able to search the HML regimes after revision on the pulse counting rules. However, searching QS and QML regimes seems beyond its capacity.

In 2015, by detecting a discontinuous jump in the polarization state of the laser output, Olivier et al. [55] successfully realized an automatic MLFL with a fundamental repetition rate of 81 MHz. The experimental setup is indicated in Figure 3(a) and the controllable variable is still the polarization state inside the cavity via a motorized polarization controller. The authors theoretically prove the feasibility of using single wave plate to lock the laser and simulate the discontinuous jump in the polarization state of the laser output when the laser is mode-locked. The experimental results are consistent with the theory that discontinuous jumps are detected when the status of the laser changes, as shown in Figure 3(b). Only $\langle S1 \rangle$, the first Stokes parameter, is used in the experiments whereas the same global behavior is observed for the other Stokes parameters $\langle S2 \rangle$ and $\langle S3 \rangle$. This study is rather novel in AML domain for its creative discrimination for the mode-locking regime. However, the authors did not discuss the polarization change of the laser output when the laser enters into other pulsation regimes (i.e., HML regimes and QS regimes) which may influence on the correct discrimination of the FML regime. In the simulation, this question is circumvented by setting the pump power to the minimum value for sustaining a single pulse.

Later in 2017, Shen et al. [56] further improved their automatic MLFL design as shown in Figure 4(a). The laser has a repetition rate of 62.5 MHz and no manual polarization controller is needed inside the cavity and all the three channels (i.e., X, Y, Z) of EPC are utilized rather only one channel in their previous research. The largest change of the design is the pulse counter part. In their previous research, only one counter is used but here they use six counters simultaneously as shown in Figure 4(b). In order to precisely acquire the repetition rate of the current state, six counters have different counting durations. Therefore, the FML regime can be correctly discriminated from various regimes including the continuous wave (CW) state, QS regimes, QML regimes and multi-pulsing regimes. The FPGA drives the DAC to sweep the three channels of the EPC one by one until the laser is mode-locked. To achieve fast start-up of AML, the three channels of the EPC are scanned at different temperatures of the fiber laser. The populations (i.e., the controlling voltages of the EPC) leading to the FML regime are illustrated in Figures 4(c)–(f) for different temperatures of the fiber laser. This study does cover the main drawbacks

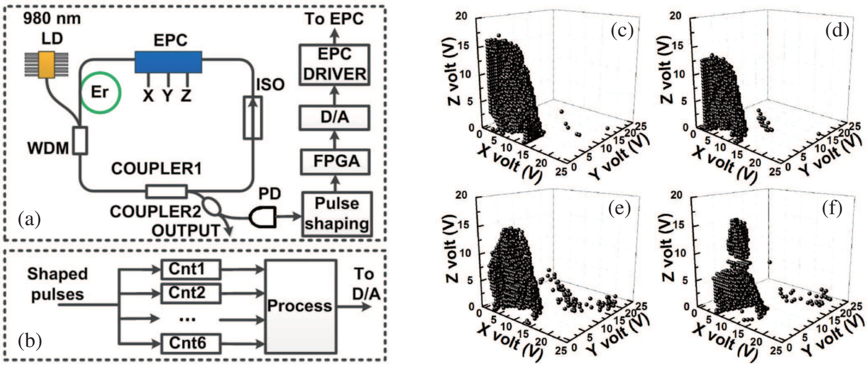

Figure 4 (Color online) (a) The experimental setup of the proposed self-tuning MLFL in [56]; (b) the pulse counter part consists of six counters; the populations of the FML regime of the laser at (c) 20°C; (d) 30°C; (e) 40°C; (f) 50°C. Reprinted with permission from [56] @Copyright 2017 IEEE.

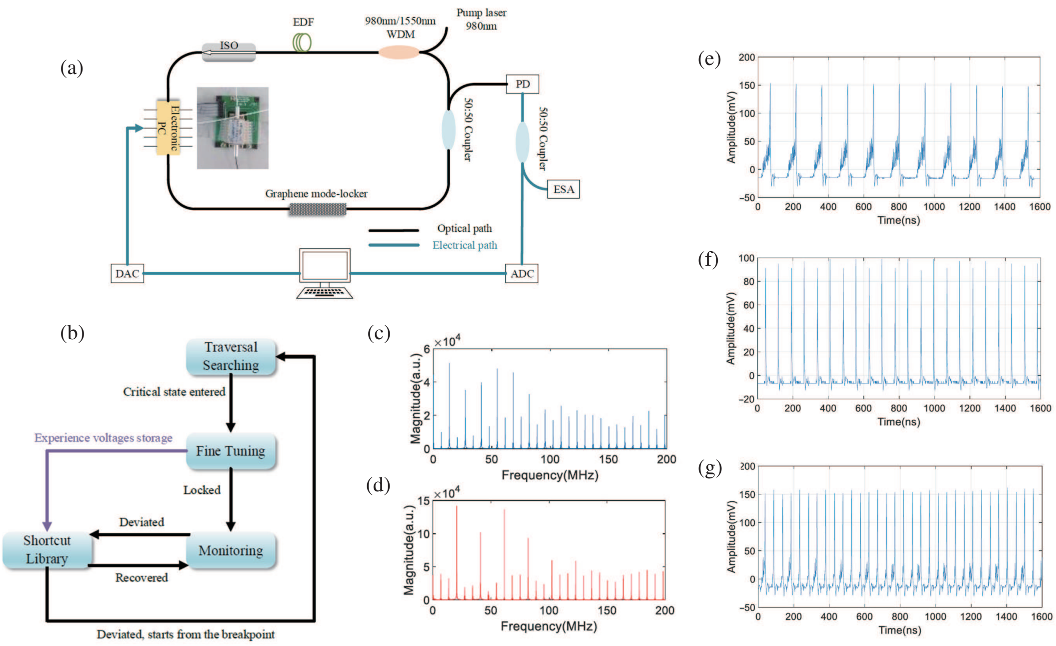

Figure 5 (Color online) (a) The experimental setup for programmable and fast-switchable passively HML fiber laser in [57]; (b) simplified traversal algorithm for AML; (c) FFT result of the second-order HML regime; (d) FFT result of the third-order HML regime. The temporal pulse train of (e) the FML regime, (f) the second-order HML regime and (g) the third-order HML regime. Reprinted with permission from [57] @Copyright 2018 Optical Society of America.

of its previous version [52]. However, there are still some improvement that could be made. For instance, the initial lock time is so long (a few minutes) because of the transversal scanning of the polarization state. The birefringence could be influenced by not only temperature but also other features like strains. Therefore, the fast start-up of AML via collecting the polarization setting under different temperatures may not always have a good performance in practical utilizations.

We achieve an automatic MLFL with the ability of automatically searching for multiple pulsation regimes containing the FML regime, the second-order HML regime and the third-order HML regime [57]. Through recording the experienced voltages leading to different pulsation regimes, the laser can switch among these pulsation regimes. The laser setup is illustrated in Figure 5(a), where the graphene mode-locker serves as both polarizer and saturable absorber. The electronic feedback setup is simplified by replacing the complex pulse shaping circuits with an ADC and a computer is used as the control center. A simplified traversal algorithm is proposed as shown in Figure 5(b) to search for the desired pulsation regime owing to the enormous polarization space (i.e., the EPC is controlled through 4 DC voltages

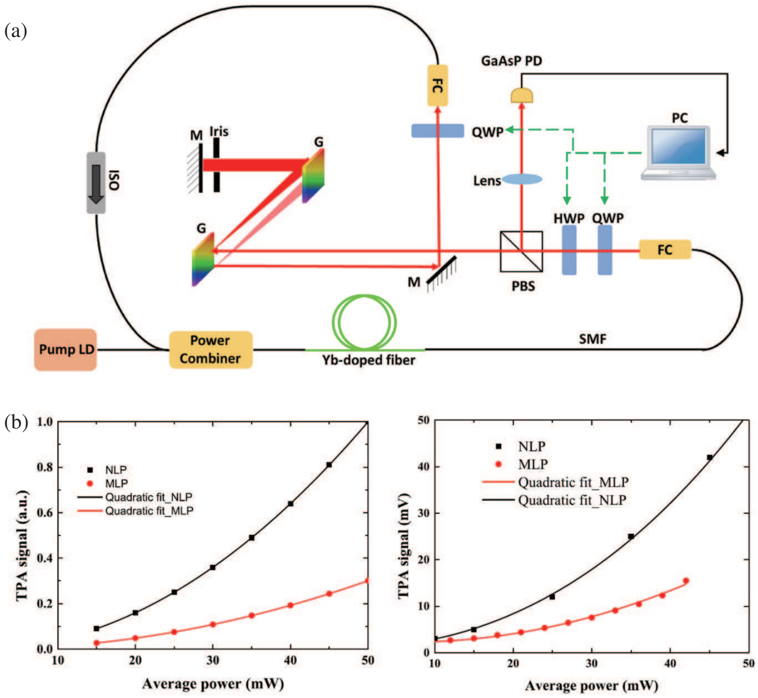

Figure 6 (Color online) (a) The experimental setup for automatically generating NLPs or mode-locked pulses in a Yb-doped fiber laser in [58]; (b) for both the NLP and the FML regime, the theoretical (left) and experimental (right) quadratic relation between the intensity of 2PA signal and the average power. Reprinted with permission from [58] @Copyright 2018 IEEE.

thereby forming a 4-dim parameter space). During searching, a shortcut library is established to record the experienced voltages leading to different pulsation regimes for fast locating on the desired pulsation regime after turning on (i.e., short initial lock time), recovering back to the desired pulsation regime when the laser deviates from the desired pulsation regime (i.e., detachments happen) and fast switching among multiple pulsation regimes. The discrimination for the FML regime is still based on pulse counting. We propose the preliminary discrimination criteria for HML regimes. By fast Fourier transfer (FFT) on temporal pulses of HML regimes, we found that for the nth-order HML regime, the amplitude of the nth spectral component is the largest among all the spectral lines as shown in Figure 5(c) and (d). Therefore, except for the pulse counting, the extra discrimination criterion for the nth-order HML regime is to verify whether the nth spectral line is the largest among all the spectral lines in frequency domain. The laser has a repetition rate of 6.85 MHz and the temporal waveforms of the searched FML regime, the second HML regime and the third HML regime are demonstrated in Figures 5(e)–(g), respectively.

Wu et al. [58] achieved automatic generation of NLPs [74–76] and the FML regime using electrical polarization control in a Yb-doped NPE-based MLFL. The experimental setup is shown in Figure 6(a). The discrimination between NLPs and the FML regime is based on the difference of 2PA signal intensity. The 2PA signal intensities induced by NLPs and the FML regime are both simulated theoretically (the left of Figure 6(b)) and measured in experiments (the right of Figure 6(b)). It is obvious that the 2PA signal induced by NLPs is much stronger than that of the FML regime. By using the 2PA signal of a GaAsP photodiode as the feedback signal, NLPs and the FML regime can be discriminated. The FML regime usually can be generated at low pump power and the NLPs occurs at higher pump powers. Therefore, automatic generation of NLPs and the FML regime is realized. However, the 2PA signals induced by other pulsation regimes are not discussed in their research.

3 AML enabled by optimization algorithms

To address the inefficiency of the traversal algorithm employed in the early stage of AML techniques,

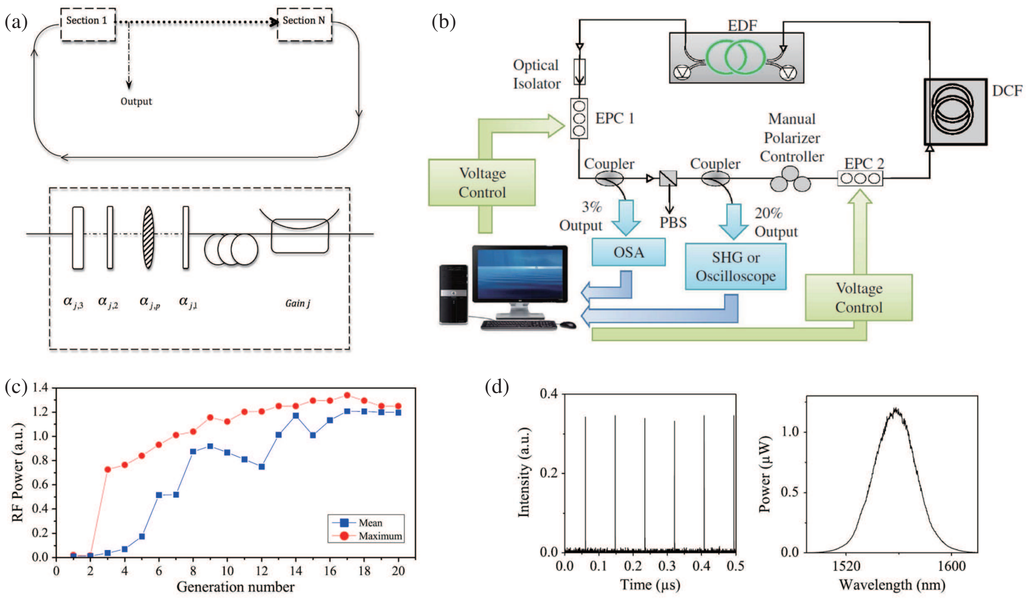

Figure 7 (Color online) (a) Configuration of the ring cavity laser system that contains multiple NPR sections (upper) in [59] @Copyright 2013 Optical Society of America. (b) The experimental setup for locking an NPR-based MLFL through an evolutionary algorithm in [60]; (c) convergence of the average (squared blue points) and best (red round points) fitness in the EA [60]; (d) the temporal pulse train (left) and the optical spectrum (right) of the FML regime found by the EA [60]. Reprinted with permission from [60] @Copyright 2015 Optical Society of America.

optimization algorithms are introduced into AML techniques to accelerate the solutions searching process in a tremendous parameter space. The genetic algorithm (GA), a classic global optimization algorithm which was inspired by the evolution of living organisms [77], is very popular among AML techniques [59–65,67]. Besides, we have proposed the human-like algorithm (HLA) powering the first real-time intelligent programmable MLFL [66]. AML lasers enabled by optimization algorithms substantially improve the efficiency of searching the solutions corresponding to the desired pulsation regimes.

In 2013, Fu et al. [59] used the GA to optimize multiple NPR filters, as shown in Figure 7(a), so as to enhance the single pulse energy of a MLFL in a theoretical simulation. The simulation demonstrates that the single pulse energy can be effectively enhanced by using the GA to properly set multiple NPR filters thereby circumventing and suppressing the multi-pulsing instabilities. In this study, for the first time, the GA is utilized in AML techniques.

The first experiment demonstration using the evolutionary algorithm (EA) to achieve AML was performed by Andral et al. [60] in 2015. Technically, the GA is a branch of the EA. The EA used in this research seems to be the GA because many terminologies of the GA including genes, an individual and population appear in this paper. The experimental setup is shown in Figure 7(b). Two EPCs and one manual polarization controller are used to control the polarization inside the cavity. Each EPC is driven by three voltages and EA is to optimize the six voltages applied on two EPCs to automatically lock the laser. First, a fitness function is proposed to be the second-harmonic generation (SHG) signal produced in a nonlinear beta BaB2O4 (BBO) crystal at the cavity output. The FML regime can produce strong SHG signal. Therefore, by consistently optimizing six voltages applied on EPCs to enlarge the SHG signal, the laser will finally be mode-locked. However, using the intensity of the SHG signal as the fitness function performs not well enough in discriminating the desired FML regime and the QML regime. The QML regime could emerge in the middle of the EA optimization. To address this problem, the intensity of the free space range (FSR) RF spectral component acquired via FFT of the temporal waveforms becomes the new fitness function. By doing so, the QML regime can be filtered. The convergence of EA using the new fitness is shown in Figure 7(c). The temporal pulses and optical spectrum of the searched FML regime are demonstrated in Figure 7(d). Hereafter, based on the same setup, an auto-setting MLFL is achieved by the same team which is capable of automatically locking onto the FML regime and HML

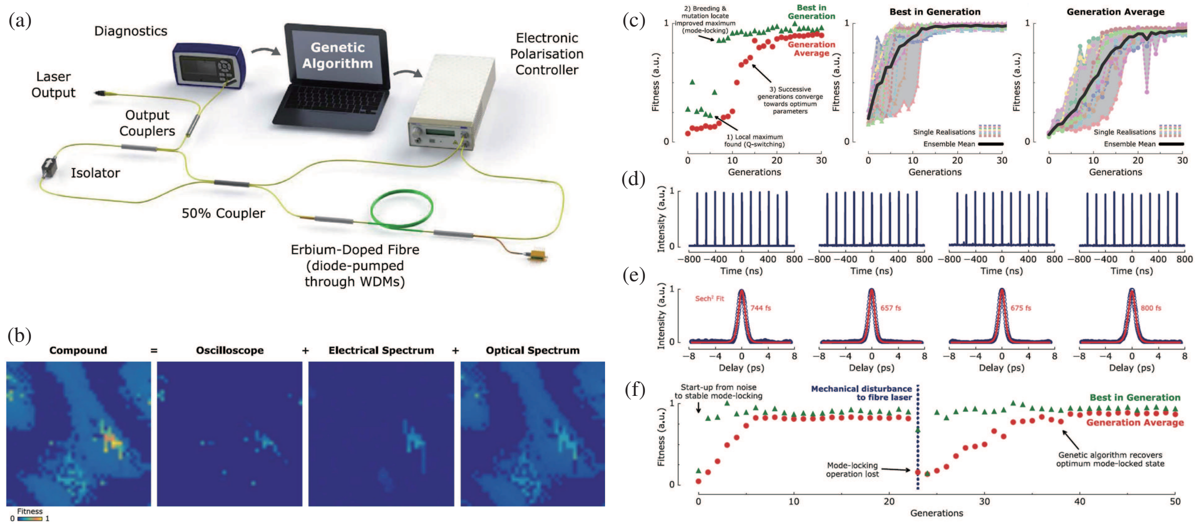

Figure 8 (Color online) (a) The experimental setup of the propose in 'smart laser' in [62]; (b) fitness map (x and y axes are QWP1 and QWP2 angle, respectively, swept through 180°), the compound fitness function consists of three components; (c) convergence of fitness for single realization (left), convergence of maximal (middle) and average fitness values over ten realizations (right); the FML regime after four consecutive realizations of the GA: (d) temporal pulse train, (e) autocorrelation traces, (f) after the laser is mechanically perturbed, fitness evolution indicating the GA recovers optimum mode-locking. Reprinted with permission from [62] @Copyright 2016 Springer Nature.

regimes using the EA [61]. The nth-order HML regimes searching relies on a new fitness function based on FFT analysis shown as follows:

$$M = \frac{A(n\mathrm{FSR})}{\frac{\sum_{i=1}^{n-1} A(i\mathrm{FSR}) + \sum_{i=n+1}^{2n-1} A(i\mathrm{FSR})}{2n-3} + C}, \tag{1}$$

where A is the amplitude of the RF component and C is a constant of the order of the noise floor, to limit noise perturbations. These researches are of significance but the initial lock time is too long (about half an hour for 12 generations of EA) because of the complexity of EA and the tremendous six-dimension solution space.

Woodward et al. [62] accomplished AML in a figure-8 MLFL using the GA as shown in Figure 8(a). Likewise, the AML is achieved by tuning the polarization state inside the cavity with an EPC, which consists of four QWPs. In this study, a compound fitness function is creatively proposed. The compound fitness is the equally weighted sum of three components extracted from the temporal waveform, the optical spectrum and the electrical spectrum. Figure 8(b) indicates the relation between the compound fitness and the three components. It should be noted that the data in Figure 8(b) are obtained by sweeping two QWPs of the EPC at a fixed resolution. The GA is effective in optimizing the compound fitness as shown in Figure 8(c) where the compound fitness nearly monotonously increases generation by generation in different presentation. The FML regimes, which are searched by four consecutive realizations of the GA, reveal repeatability as shown in Figure 8(d) and (e). Further, the GA-based automatic MLFL has the ability to resist external mechanical disturbances. As shown in Figure 8(f), the laser can recover to the FML under the direction of the GA. This study further paves the way of using the GA in AML techniques. However, the three components constituting the compound fitness are collected using large equipment including an oscilloscope, an optical spectrum analyzer (OSA) and an RF spectrum analyzer. Hence, the cost and the portability of this technique cannot be ensured in a short time. Additionally, owing to the slow data acquisition using large equipment and the complexity of the GA, the initial lock time could even raise to around 30 min which is tedious.

By using the EPC based birefringent filter [78–80] and automatic pump control, the same group realized self-tuning QS regimes in a NPR-based ring cavity laser, as shown in Figure 9(a) [63]. Under the guidance of the GA, both the central wavelength and repetition rate of the QS regime can be automatically tuned.

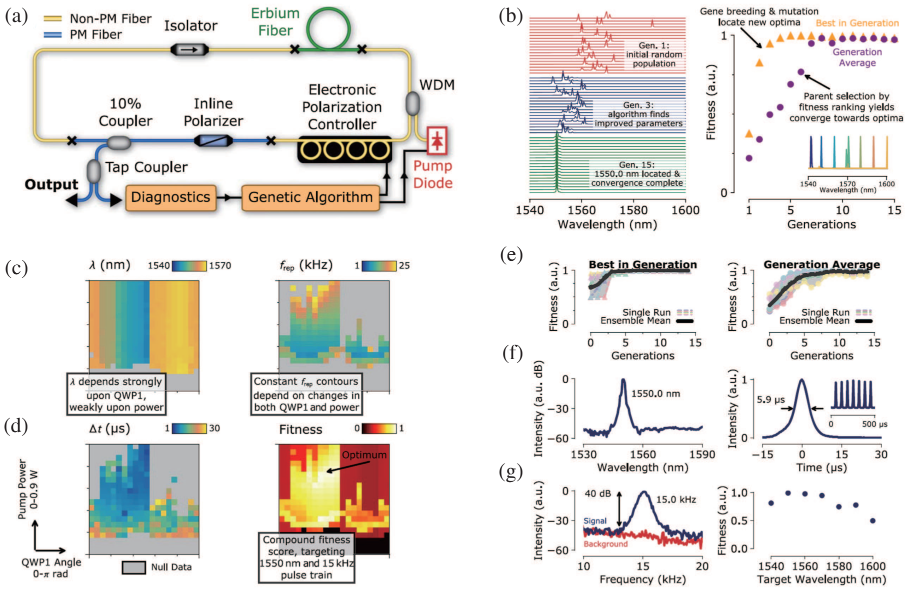

Figure 9 (Color online) (a) The experimental setup of the GA-based control of birefringent filtering for self-tuning, self-pulsing fiber laser in [63]; (b) wavelength self-tuning: visualization of spectra in different generations (left), fitness evolution (inset: obtained spectra by self-tuning indicating tuning range) (right); (c) maps of laser characteristics in relation to the QWP1 angle (x axis) and the pump power (y axis): central wavelength (left) and repetition rate (right); (d) maps of laser characteristics in relation to the QWP1 angle (x axis) and the pump power (y axis): pulse duration (left) and fitness score with targets: a central wavelength of 1550 nm and a repetition rate of 15 kHz (right), self-tuning characteristics, with targets the central wavelength of 1550.0 nm and the repetition rate of 15 kHz; (e) convergence of fitness for best fitness in each generation (left) and average fitness of each generation (right); (f) the optical spectrum (left) and the temporal pulse (right); (g) the RF spectrum (left), optimum achieved fitness when targeting variable central wavelengths under the fixed repetition rate of 15 kHz (right). Reprinted with permission from [63] @Copyright 2017 Optical Society of America.

A new compound fitness function is proposed as shown in (2)–(4) so as to achieve self-tuning of the central wavelength and repetition rate. The F_λ is established for the central wavelength tuning ($F_\lambda = 1$ is optimal). λ is the measured central wavelength through an OSA, λ_0 is the target central wavelength and $\Delta = 70$ nm is the estimated gain bandwidth.

$$F_{\text{total}} = 0.5F_\lambda + 0.5F_f, \tag{2}$$

$$F_\lambda = 1 - \frac{\lambda - \lambda_0}{0.5\Delta\lambda}, \tag{3}$$

$$F_f = 1 - \frac{f - f_0}{0.5\Delta f}, \tag{4}$$

where F_f is used to control the repetition rate. f is the measured repetition rate and f_0 is the target repetition rate. GA-based central wavelength self-tuning is shown in Figure 9(b). The target central wavelength is 1550 nm which is obtained at the 15th generation (the left of Figure 9(b)). The convergence of fitness is shown in the right of Figure 9(b) and the wavelength tuning range is 1542.2–1600.4 nm with a resolution of 0.1 nm through experiments. Maps of the laser characteristics is shown in Figure 9(c) and (d) by sweeping the pump power from 0 to 0.9 W and only one QWP of the EPC from 0 to π rad. Note that the right of Figure 9(d) is the map of compound fitness when targeting the central wavelength of 1550 nm and the repetition rate of 15 kHz pulse train. The experiment results of self-tuning the pulse train with the central wavelength of 1550 nm and the repetition rate of 15 kHz are demonstrated in Figure 9(e)–(g). The fitness convergence is shown in Figure 9(e) validating the effect of the GA. The optical spectrum (left) indicating the central wavelength of 1550 nm as targeted and the temporal pulse shape (right) are shown in Figure 9(f). The RF spectrum is shown in the left of Figure 9(g) giving the repetition rate of 15 kHz. Besides, the experiments of targeting various central wavelengths under the fixed repetition rate of 15 kHz are carried out and the optimum achieved fitness is shown in the right of Figure 9(g). The

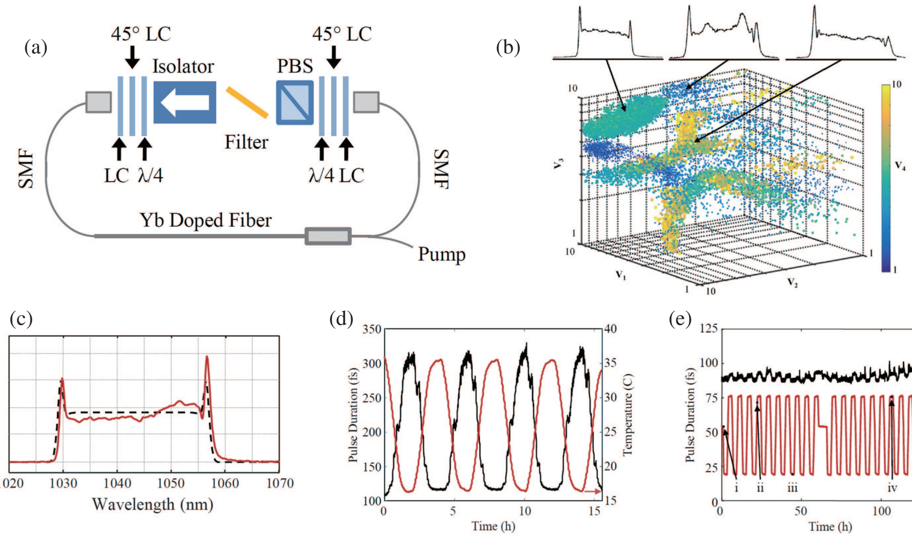

Figure 10 (Color online) (a) The experimental setup in [64]. (b) The FML regimes found through a full-range scan, demonstrating spectra for several operating points. The four control values are represented as spatial locations and the color of the marker. (c) A target ANDi spectrum (the black dashed) with a spectral width of 25 nm centered at 1043 nm and the spectrum found by the GA (the red solid) with this target. The relation between pulse width and the environmental temperature in (d) a standard no electrical-polarization-control oscillator and (e) an LC stabilized oscillator. Reprinted with permission from [64] @Copyright 2017 Optical Society of America.

optimum achieve fitness is high signifying that the QS regime with targeted parameters are successfully achieved. This research is important to the evolvement of AML techniques for two reasons. The pump power is taken consideration as a variable thereby achieving automatic pump control for the first time and the optical spectrum is controlled through an algorithm in this domain, though only some parameter of the optical spectrum that can be controlled. However, this research shares the same flaws (high cost, poor portability and long initial lock time) as the previous one [62].

Then, Winters et al. [64] successfully achieved AML in an all-normal dispersion (ANDi) MLFL using electrical polarization control and the GA. The laser setup is shown in Figure 10(a). The electrical polarization control is realized through two parts. Each part consists of two LC variable phase retarders which are controlled by voltages and a fixed QWP. Hence, the parameter space of polarization is four-dimension. Figure 10(b) demonstrates the searched FML regimes during scanning the four LCs. The fitness function is the coefficient of determination, R2 [81], between the measured optical spectrum and the target optical spectrum which reveals the spectral similarity between these two spectra. Figure 10(c) indicates a spectrum of the FML regime is found (the red solid) using the GA and the proposed fitness function when targeting an ideal ANDi spectrum (the black dashed) is defined by a central wavelength of 1043 nm and a spectral width of 25 nm. Since the laser is operating near the desired point in many cases, the desired regime can be found quickly using a local optimization algorithm. The hill climbing algorithm is used to deal with the detachments (i.e., the laser detaches from the desired regime) from the FML regime. By doing so, the stability of output pulse duration is substantially promoted as shown in Figure 10(d) and (e). Further, the FML regime can be reached after 9 generations using a population size of 50 in about 90 s via the GA and the laser can recover back to the FML regime from detachments within 30 s using the hill climbing algorithm.

Ryser et al. [65] achieved the control of an ANDi NPR-based MLFL working under different regimes including the FML regime, the single CW state and the dual CW state by combining electrical polarization control and the GA. The proposed self-tuning laser is indicated in Figure 11(a). The electrical polarization control is realized by introducing three motorized wave plates into the cavity. The pulse amplitude jitter is chosen to be the fitness function of the GA shown as follows:

$$\Delta E/E \propto \sqrt{(P_C/P_A)_1}, \tag{5}$$

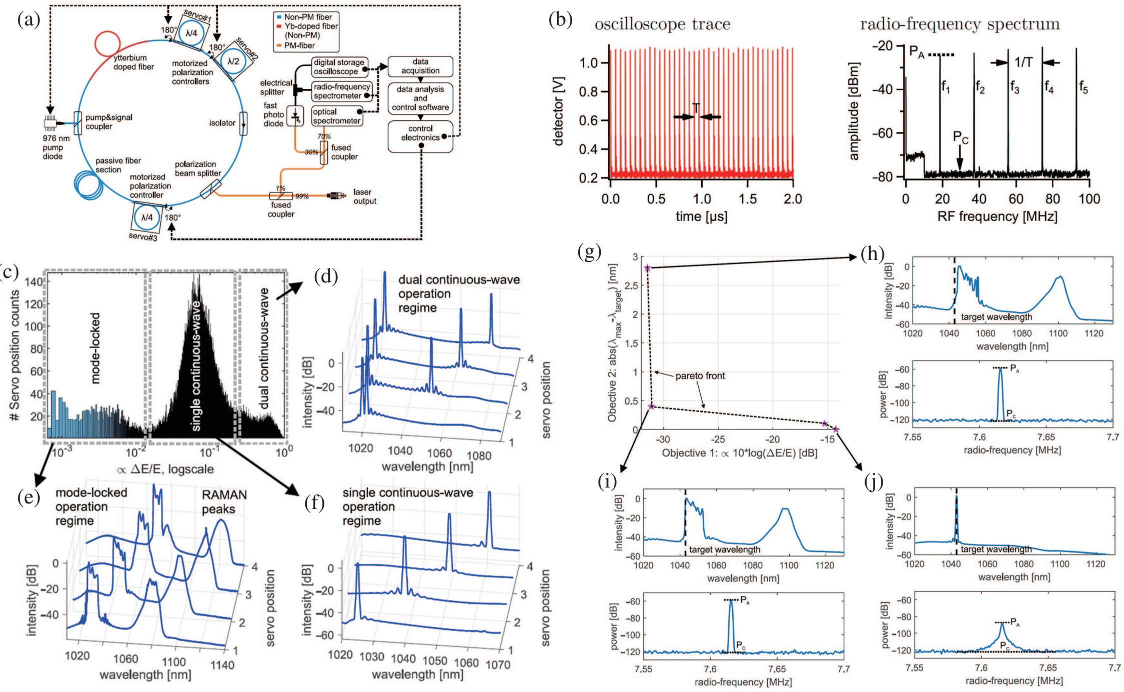

Figure 11 (Color online) (a) The experimental setup of the self-tuning fiber laser in [65]. (b) The oscilloscope trace (left) and the RF spectrum (right) of the FML regimes. (c) The distribution histogram of pulse amplitude jitter from a full polarization scan. (d) Multiple laser lines in the CW state appear in the spectral at large jitter values. (e) The laser operates in the FML regime at the lower end of jitter values. (f) The laser operates in the single CW state at the largest peak in the histogram (jitter values of 0.1), two objective optimization. Objective 1 is the pulse amplitude jitter and objective 2 is the absolute value of the difference between the measured wavelength with maximum intensity and the target wavelength. (g) Distribution of various regimes on a map of objective values. (h) Operation regime meets objective 1, but not objective 2. (i) Operation regime meets both objective 1 and 2. (j) Operation regime meets objective 2, but not objective 1. Reprinted with permission from [65] @Copyright 2018 SPIE.

where E is the pulse energy, P_A is the amplitude of the fundamental frequency in the RF spectrum and P_C is the noise in the RF spectrum as shown in the right of Figure 11(b). The subscripts of the brackets are the order number of the harmonics in the RF spectrum, where the subscript 1 is the fundamental frequency. The laser is approaching the FML regime when the pulse amplitude jitter is decreasing. The distribution histogram of the pulse amplitude jitter is established and shown in Figure 11(c) via a full polarization scan. The laser operates in the dual CW state at large jitter values around 1 as shown in Figure 11(d). Figure 11(e) demonstrates that the laser operates in the FML regime at small jitter values around 0.001. At middle jitter values around 0.1, the laser operates in the single CW state as shown in Figure 11(f). Additionally, multi-objective optimization is achieved as well. By using a compound fitness which is composed of the pulse amplitude jitter (objective 1) and the absolute of the different between the measured wavelength with maximum intensity and the target wavelength (objective 2), an FML regime is achieved whose wavelength with maximum intensity can be self-tuned. Distribution of various regimes on a map of objective values in a multi-objective optimization is shown in Figure 11(g). Figure 11(h) shows the operation regime that fulfills well objective 1, but not objective 2. Figure 11(i) shows the desired operation regime that fulfills both objective 1 and 2 quite well. Figure 11(j) shows the operation regime that fulfills well objective 2, but not objective 1. Similar as the previous studies, using large equipment including an oscilloscope, a RF analyzer and an OSA for feedback data acquisition are very time-consuming and costly. Simultaneously, the lack of portability is not ideal for industrial applications. Additionally, using a PC as the computation center with no doubt exacerbates the time consumption during the optimization.

Recently, we achieved the first real-time intelligent programmable MLFL as shown in Figure 12(a) [66]. The laser is able to automatically lock onto various operation regimes including the FML regime, the

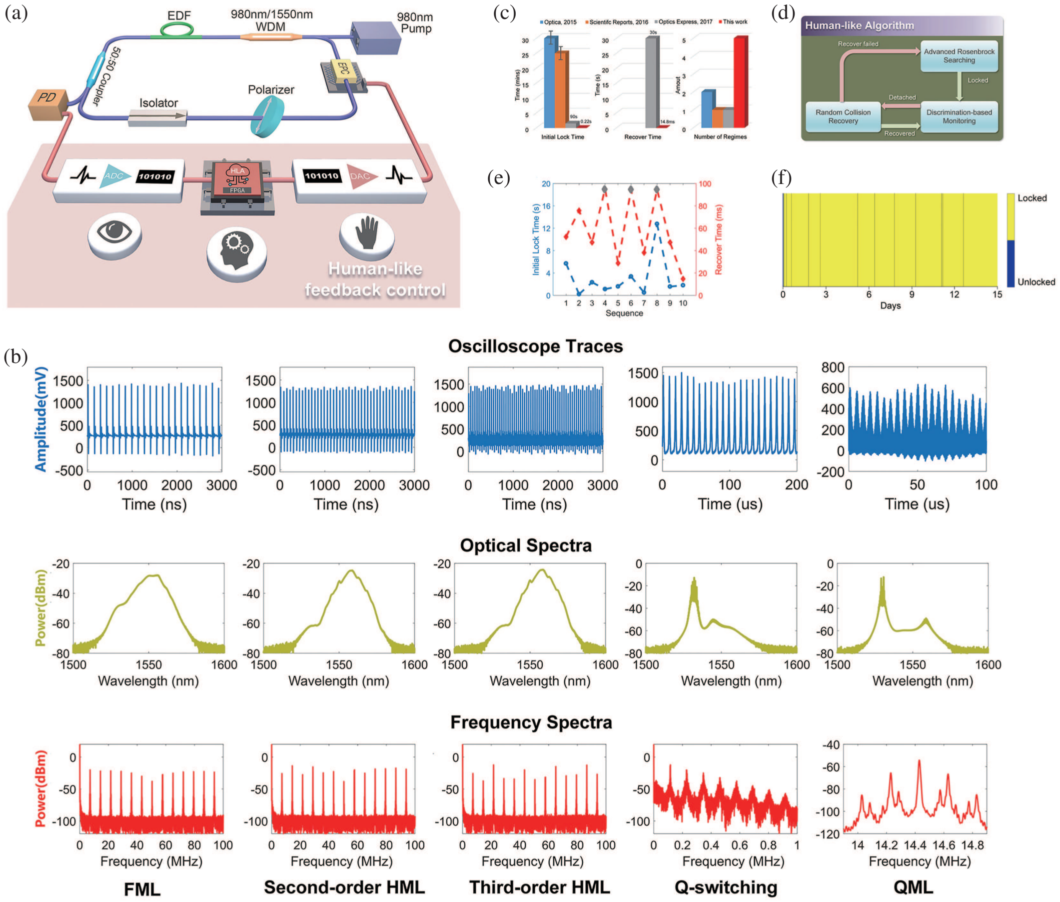

Figure 12 (Color online) (a) Real-time intelligent MLFL in [66]; (b) operation regimes, from left to right respectively shows the FML, the second-order HML, the third-order HML, the QS, and the QML operation regimes; (c) comparisons over initial lock time, recovery time, and number of regimes between recent AML studies and our study; (d) schematic of human-like algorithm; (e) time consumption of the FML regime on initial mode-locking (the blue dashed line) and recovery (the red dashed line) over ten successive experiments; (f) a 15-day running record. Reprinted with permission from [66] @Copyright 2019 Optical Society of America.

second-order HML regime, the third-order HML regime, the QS regime and the QML regime as shown in Figure 12(b) (the richest regimes to date). Further, the laser substantially promotes the previous initial lock time and recovery time of the FML regime. The shortest starting up (from the CW state to the FML regime) costs only 0.22 s and the shorter recovery costs merely 14.8 ms as shown in Figure 12(c). The time-consuming performance is demonstrated in Figure 12(e) over ten successive experiments of the FML regime on initial mode-locking and recovery. The mean of ten initial lock times is only 3.1 s and the mean of ten recovery times is merely 58.9 ms. Moreover, a 15-day running test is performed in an open environment without any thermal-stability or vibration-protection devices and the recording is shown in Figure 12(f). The laser initially reaches the FML regime within 0.5 s. Then, 12 detachments happen in 15 days and the mean recovery time is only 31 ms. The excellent performance of the laser is contributed to the real-time implementation and the proposed human-like algorithm. As shown in Figure 12(a), the real-time circuit is composed of an ADC, an FPGA and four DACs that controls the EPC. Compared to the off-line implementations, the real-time implementation reveals a dominant advantage on the time-consuming performance. A single round feedback, which contains data sampling via ADC, algorithms running in FPGA and controlling the EPC by DACs, costs only 1 ms. On the other hand, the human-like algorithm is proposed as illustrated in Figure 12(d). The human-like algorithm mainly consists of three portions: the advanced Rosenbrock searching (ARS) algorithm, the random collision recovery algorithm, and the discrimination of each regime. The human-like algorithm starts from ARS, which is utilized to lock onto the desired regime. After locking onto the desired regime, the human-like algorithm focuses on

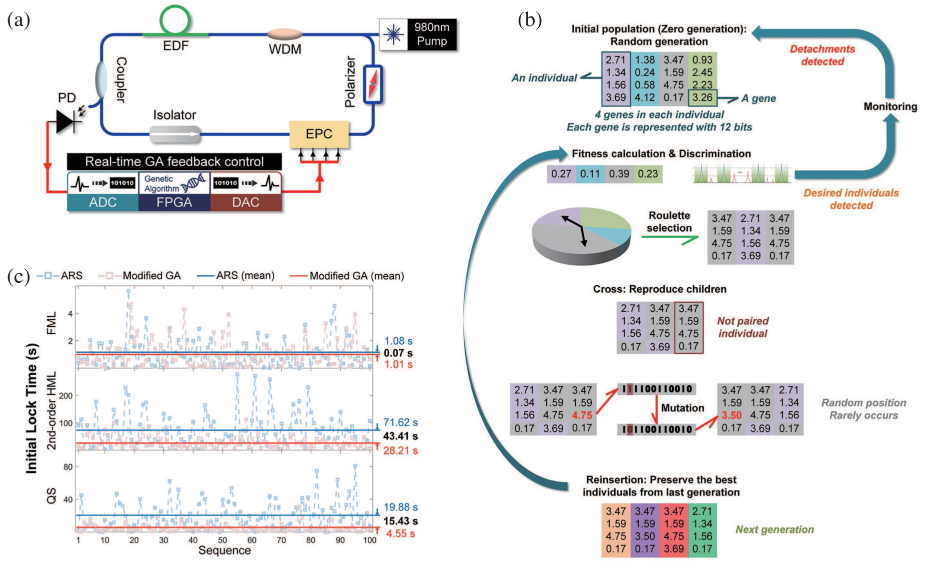

Figure 13 (Color online) (a) GA-based real-time automatic MLFL setup in [67]; (b) the flowchart of the proposed modified GA; (c) time consuming performance comparison between the ARS and the modified GA. Reprinted with permission from [67] @Copyright 2020 IEEE.

discrimination-based monitoring (unless a detachment is detected). Random collision recovery attempts to pull the laser back on track afterward. The human-like algorithm goes back to the monitoring process if the recovery is successful. Otherwise, restarting ARS is necessary to anchor a new desired point. This software scheme is denoted as the human-like algorithm because our proposed algorithm has many features in common with human logic and behaviors in the manual mode-locking process and the ARS process is somewhat an analogy of human behaviors in polarization tuning. To achieve the automatic search of various regimes, a set of objective functions and discrimination criteria for various regimes are established. Only the waveform sampled by a low-speed ADC is required in the proposed discrimination criteria so large equipment like oscilloscopes, OSAs and RF spectrum analyzers are not required as in the previous research therefore significantly reducing the cost and enhancing the portability. Through combining the real-time implementation and the human-like algorithm, we successfully address some everlasting drawbacks in AML domain including long time consumption, the lack of portability owing to the use of large equipment and the accompanying high cost. Moreover, programmable various regimes output enhances the flexibility of the laser endowing in a promising future in both research and industrial applications.

Combining the proposed discrimination criteria and the traditional GA, we propose a modified GA to further improve the time-consuming performance of the automatic MLFL [67]. The experimental setup is quite similar with our previous research as shown in Figure 13(a). The modified GA is illustrated in Figure 13(b). The fitness functions for various regimes follow the objective functions in our previous research as well. The core idea of the modified GA is a discrimination operation to judge whether or not the current waveform reaches the desired regime is performed simultaneously during the fitness calculation and the algorithm stops searching immediately when the desired regime is detected, thus significantly reducing the algorithm's running time (skipping the rest generation calculations in the GA). The laser then sequentially enters into the monitoring phase based on the discrimination operation. When detachment is detected, the laser will automatically recover to the desired regime by launching the modified GA again. The experimental results of time-consuming performance comparison between the modified GA and the ARS are shown in Figure 13(c). To ensure the validity of the comparison results, the comparison experiments are conducted using an identical cavity at nearly the same period. A timer inside FPGA with a time resolution of 3 ns is used. When searching the FML regime, the two algorithms have nearly the same time-consuming performance. However, when searching rare regimes including the second-order HML regime and the QS regime, the modified GA reveals huge advantage over the ARS on

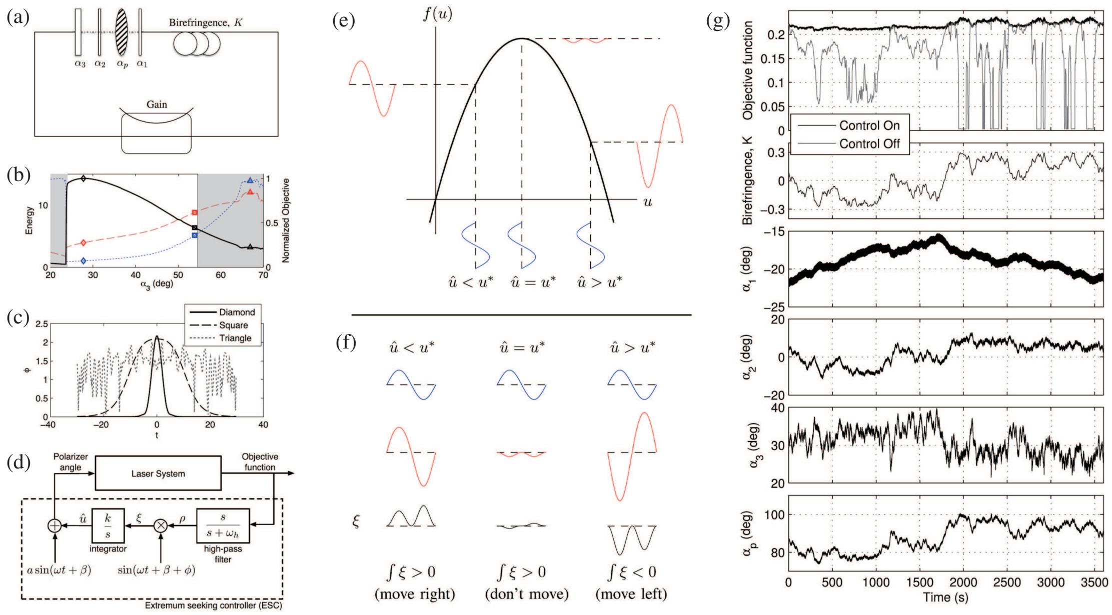

Figure 14 (Color online) (a) Abstract model of NPR-based MLFL contains two quarter-wave plates (α_1 and α_2), one half-wave plate (α_3), one passive polarizer (α_p), gain and the birefringence parameter K in [68]; (b) the objective function (the black solid), energy (the red dashed), and kurtosis (the blue dotted) as a function of half-wave plate angle α_3; (c) energy of the waveforms as a function of time for the cases shown in diamond, square, and triangle; (d) single-input, single-output ESC; the principle of ESC; (e) illumination of sinusoidal perturbation to the input $\hat{u}$ close to an optimal value u^*; (f) the curves ξ is given by the input and high-pass filtered outputs; (g) multi-parameter ESC with a varying birefringence. Reprinted with permission from [68] @Copyright 2013 IEEE.

the time-consuming performance. This is contributed to the inherent powerful global optimization ability of the GA. Moreover, the time consumption variation over 100 measurements of the ARS is greater than that of the modified GA (particularly in the second-order HML regime and QS regime cases) owing to the ARS's sensitivity to the initial point. Overall, the proposed modified GA exhibits a better time-consuming performance than the ARS. So far, this study reveals the best time-consumption performance on the initial locking. Various mode-locking regimes can be searched and programmable based on the discrimination criteria, while the cost and portability of the MLFL can also be guaranteed, therefore almost resolving the long-standing dilemma of NPR-based MLFLs.

4 AML enabled by machine learning

Recently, owing to the exponential increase of calculation capacity of computers, machine learning based deep learning has extensively utilization in various disciplines including well-known 5G [82], autonomous driving [83] and some unusual applications like sentiment analysis [84]. Thus, there is no much surprise that machine learning [85–87], as one of the hottest techniques, has also been applied in AML domain [68–72]. Researches in this area are mainly pushed forward by the team of J. Nathan Kutz from the University of Washington, Seattle.

Later in 2013, the team demonstrated numerical simulations where extremum-seeking control (ESC) algorithm is used to simultaneously obtain and maintain the high-energy FML regime in a NPR-based MLFL numerical model as shown in Figure 14(a) [68]. The ESC is actually a local optimization algorithm [68], not an algorithm of machine learning. The reason of this research is introduced in this section is that the ESC-based AML technique is a foundation of their future researches. The objective function is dividing the energy by the kurtosis of the Fourier spectrum of the waveform. The relationship among the objective function, energy and the kurtosis versus half-wave plate angle α_3 is illustrated in Figure 14(b). Combining with Figure 14(c), it is obvious that the highest objective value corresponds to a high-energy FML regime which validates the effectiveness of the objective function. Figure 14(d)

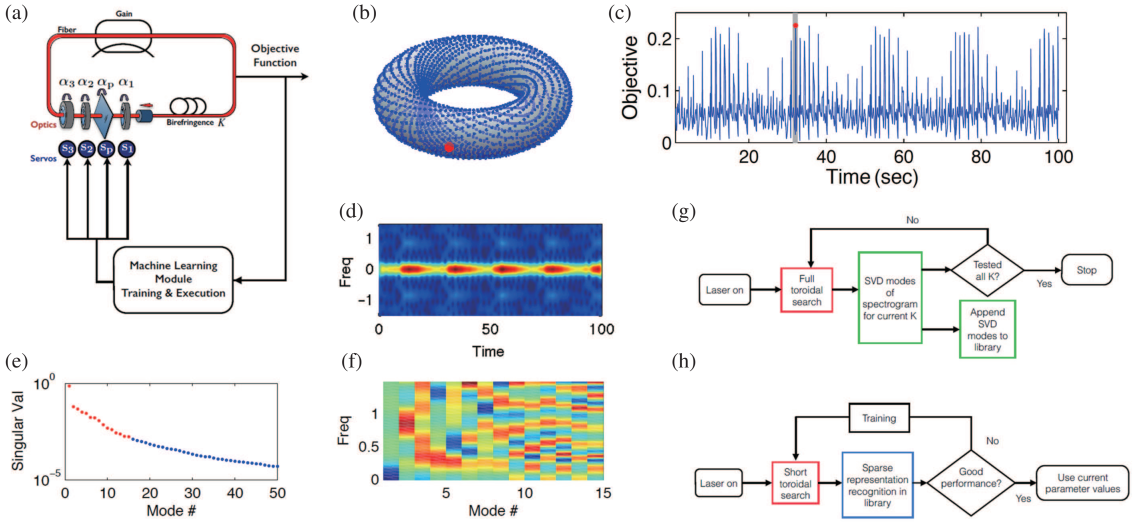

Figure 15 (Color online) (a) The simulation setup in [69]; (b) 2-torus of the half-wave plate angle α_3 and the polarizer angle α_p with sample points shown (dots) at a sampling rate of 20 Hz (the red point: the global optimum); (c) the time-series of the corresponding objective function (the red point: the global optimum); (d) spectrogram of the time series; (e) singular values obtained by SVD, the largest 15 singular values are plotted in red; (f) SVD modes of the largest 15 singular values; (g) illustration of training algorithm; (h) illustration of execution algorithm. Reprinted with permission from [69] @Copyright 2019 Optical Society of America.

demonstrates the schematic of the single-input, single-output ESC. The ESC is an adaptive control law that finds and tracks local maxima of an objective function by gradient probing, which is sinusoidally varying a set of input parameters and measuring the consequent variation of the objective function. The concrete principle is indicated in Figure 14(e) and (f). After high-pass filtering on the objective function under the input sinusoidal perturbation to eliminate the slow external disturbances, a demodulated signal ξ is obtained by multiplying the filtered output by the input perturbation. When the integration of ξ is positive (negative), the input $\hat{u}$ is smaller (larger) than the optimal value u^*. $\hat{u}$ is closer to u^* when the integration of ξ is near zero. The simulation result using the ESC in the laser with a varying birefringence is shown in Figure 14(g). With the ESC, the objective function value nearly maintains the largest value corresponding to the high-energy FML regime.

Then, they used machine learning and sparse representation to successfully classify birefringence in MLFLs in a numerical simulation [69]. The simulation model is shown in Figure 15(a). Different from the previous one [68], a machine learning model is applied as the feedback core. In the training process, a library is established, which includes the mapping between various cavity birefringence values and the optimal solution of the servo voltages applied on the wave plates and the polarizer. First, for each birefringence value, a full toroidal search is performed to locate the optimum as shown in Figure 15(b) and (c). It should be noted that the objective function follows the previous one [68]. A unique spectrogram shown in Figure 15(e) for the current birefringence value is obtained via performing a Gabor transform on the time series of objective function shown in Figure 15(d). Then, a singular value decomposition (SVD) reduction on the spectrogram is performed by keeping the first m modes in the SVD result as indicated in Figure 15(f) and (g). The current birefringence is now represented by the m modes. In the execution process, first, a short toroidal search is executed to get a time series of objective function. The m modes of the unknown birefringence value can be obtained through a Gábor transform and an SVD reduction. Then, an L1-norm minimization is performed based on the m modes of the unknown birefringence value and the library. The L1-norm minimization produces a sparse vector, i.e., only a small portion of the elements are non-zero. The non-zero elements of the sparse vector act as a classifier (indicator function) for identifying which sub-library the current birefringence falls into. This method is termed as sparse representation. The training process and the execution process are illustrated in Figure 15(h) and (i) respectively. After the birefringence is recognized, the optimal solution of the servo voltages is readily

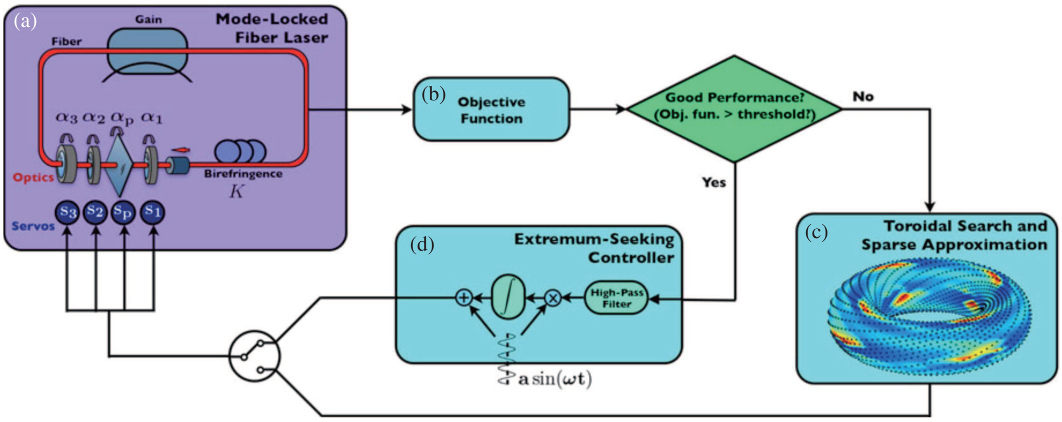

Figure 16 (Color online) Schematic of the self-tuning fiber laser in [70]. (a) The laser cavity; (b) the objective function is dividing the energy by the kurtosis of the Fourier spectrum of the waveform; (c) the toroidal search and sparse approximation; (d) the ESC. Reprinted with permission from [70] @Copyright 2014 IEEE.

acquired through the library.

Further, through combining the ESC and the machine learning based birefringence classification, they proposed a self-tuning fiber laser based on numerical simulations as indicated in Figure 16 [70]. In the training process, a library including the mapping between various cavity birefringence values and the optimal solution of the servo voltages applied on the wave plates and the polarizer is established using the full toroidal search, the Gábor transform and the SVD reduction. In the execution process, the current birefringence of the laser cavity is characterized by a short toroidal search and classified with the sparse representation. The optimal solution then is given by the library. The ESC is to address the small performance variation brought by environmental disturbances. However, if the operation regime of the laser does not have the expected performance (the objective function value is lower than the threshold) after the optimal solution is applied owing to a large disturbance, the algorithm goes back and performs another short toroidal search to re-identify the birefringence through a sparse classification as illustrated in Figure 16.

Recently, they released an update of the self-tuning laser by integrating a deep learning [88] architecture with model predictive control (MPC) [89] based on numerical simulations [72]. The schematic of the self-tuning fiber laser is shown in Figure 17(a) and the previous objective function is inherited to assess the operation regime of the laser. Recent studies have shown that a variational autoencoder (VAE) is able to learn a meaningful structured latent space [46, 47]. Since the birefringence cannot be directly measured, a VAE (i.e., the inner loop in Figure 17(a)) is used to infer a representation of the birefringence from its latent space. Figure 17(b) shows the performance of the VAE. The representation of the birefringence inferred by the VAE (green line) successfully tracks the true birefringence (blue line). Then, a fully-connected neural network (NN) is used to learn the mapping between the representation of the birefringence and optimal control inputs (i.e., the wave plates and the polarizer). The MPC has been used in process control since the 1980s. In recent years, it has emerged as a leading control architecture owing to its flexible and robust performance on strongly nonlinear systems [89]. Here, the MPC is utilized to fast regulate the laser through predicting future optimal control inputs. The MPC (i.e., the outer loop in Figure 17(a)) is achieved by a recurrent neural network (RNN). In the beginning, the inner loop consisting of a VAE and a fully-connected NN operates to obtain adequate historical data, which contains both the cavity states (i.e., the representation of the birefringence) and the corresponding optimal control inputs. According to the sequence of the historical cavity states, the MPC is used to predict the optimal control inputs for the next N time steps. However, if the prediction error exceeds a certain threshold, then the inner loop will be initialized again to stabilize the laser. Performance of the system under significant random changes in birefringence over time is demonstrated in Figure 17(c). The objective function with deep learning control maintains a large value indicating the laser is operating under a high-energy pulsation regime.

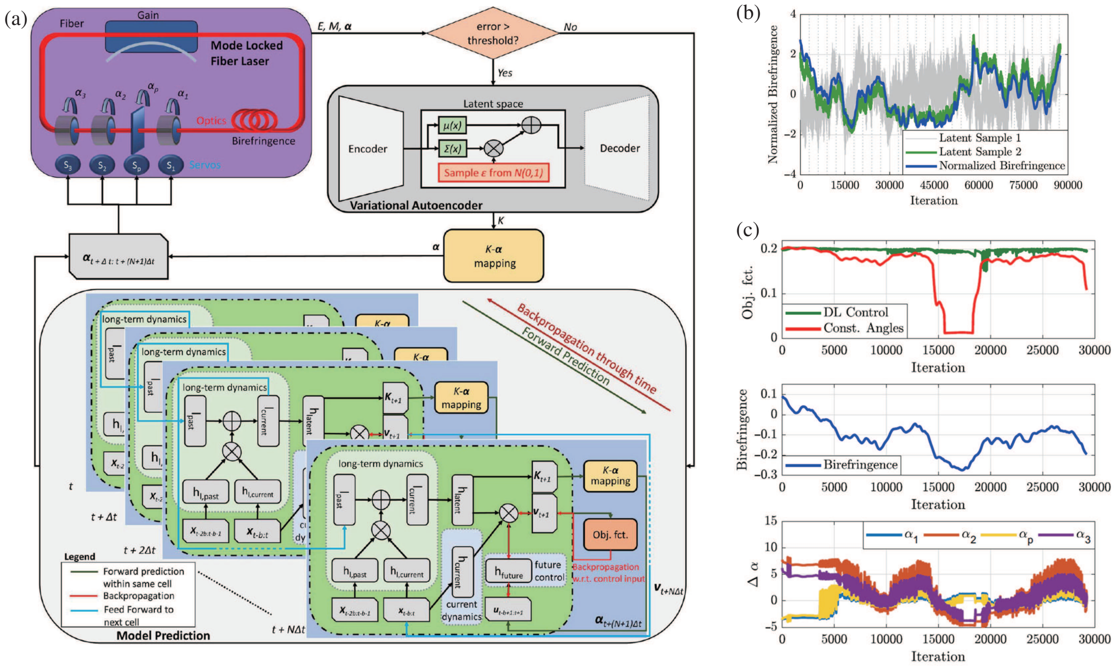

Figure 17 (Color online) (a) Schematic of the deep learning controller in [72]; (b) comparison between the true birefringence (the blue line) and the samples from the latent space of two dimensional VAE's; (c) performance of the system despite significant random changes in birefringence over time. Reprinted with permission from [72] @Copyright 2018 Optical Society of America.

These studies of using machine learning and deep learning to achieve AML demonstrated a new algorithmic perspective to address the polarization tuning problem in NPR-based MLFLs. In the future, using appropriate machine learning and deep learning algorithms to achieve AML may be a more efficient method as the development of calculation ability. However, for now, these studies are based on numerical simulations only. Although with a good theory guiding data generation in simulations, there are still some doubts on the validity of these methods being used in the real experiments.

5 AML: perspectives and applications

To facilitate the applications of AML techniques in commercial MLFLs, it is significant to select the most appropriate algorithm for AML through comparing the time-consuming performance (including initial lock time and recovery time) and the stability of the machine learning algorithms and various optimization algorithms in the experimental field. For now, the machine learning and deep learning algorithms enabled self-tuning MLFLs are proposed based on numerical simulations but lack of experimental demonstration [68–72]. Hence, it is urgent to experimentally realize the machine learning and deep learning algorithms enabled AML laser. In addition, we would like to share some thoughts on how to achieve an AML laser with high performance. First, from the perspective of algorithm, we need to design objective functions which are effective and easy to calculate. Good objective functions will correctly guide the algorithm optimization thereby reducing the running time. The time complexity and global optimization ability are the two prior metrics that we should consider when designing or selecting the optimization algorithm. Second, from the perspective of hardware, real-time realizations, where FPGAs or MCUs are used as computation center, ADCs and DACs are used for data acquisition and controlling respectively, are strongly recommended to achieve excellent time-consuming performance.

In order to improve the intelligence level of AML lasers, more dimensional information should be used as the feedback signal. Apart from the common temporal waveform and the electrical spectrum, the optical spectrum obtained using an OSA is also utilized in AML lasers thereby the output optical spectra of the lasers can be controlled to some extent (i.e., central wavelength tuning) [62–64]. However, using

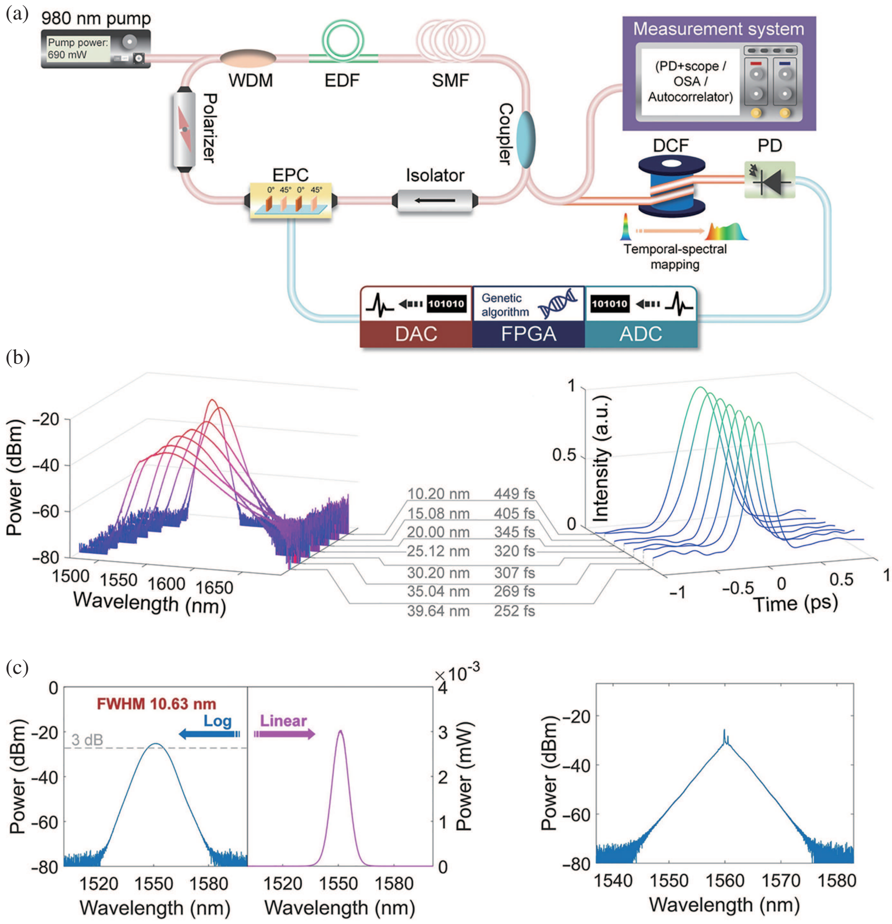

Figure 18 (Color online) (a) The time-stretch-assisted intelligent mode-locking fiber laser in [92]; (b) spectral width programming from 10 to 40 nm, showing the spectra (left) and autocorrelation traces (right); (c) spectral shape programming: the fitted hyperbolic secant spectrum (left), fitted triangular spectrum (right). Reprinted with permission from [92] @Copyright 2020 Springer Nature.

an OSA to obtain the integrated spectral information is slow and therefore cannot be used for real-time mode-locking. Combining a high-speed ADC and the time-stretch dispersion Fourier transform (TS-DFT) which builds up a mapping between the spectrum and the temporal domain pulse through a dispersive medium [90, 91], the real-time optical spectrum acquisition and analysis is possible. Recently, through this method, we achieved real-time intelligent control of mode-locked femtosecond pulses as shown in Figure 18(a) [92]. As demonstrated in Figure 18(b), the spectral width can be tuned from 10 to 40 nm with a resolution of ∼1.47 nm (the corresponding temporal pulse width can be controlled accordingly). The spectral shape can be programmed to be hyperbolic secant or triangular as shown in Figure 18(c). In addition, using this method, some other spectral features can be controlled signifying a real-time control over the spectra of MLFLs. Therefore, some interesting researches like automatic searching on soliton molecules [93, 94] become possible owing to the fast optical spectrum analysis and discrimination. The autocorrelation trace is always a very important metric to assess both the temporal durations and the pulse shapes. Likewise, the temporal features of the pulses can be controlled as well by introducing the autocorrelation trace into the feedback. For this application, the low-cost and real-time acquisition of autocorrelation trace is indispensable and needs to be solved.

On the other hand, more dimensional variables should be controlled by the algorithm in the feedback. More dimensional variables will bring an exponential increase to the solution space, where the necessity of AML techniques is more obvious and the algorithm efficiency becomes crucial. In addition to polarization, there are many other variables contributing to various regimes. Pump power, which is highly related to the pulse peak power, the unwanted multi-pulsing instabilities and the formation of HML regimes, is

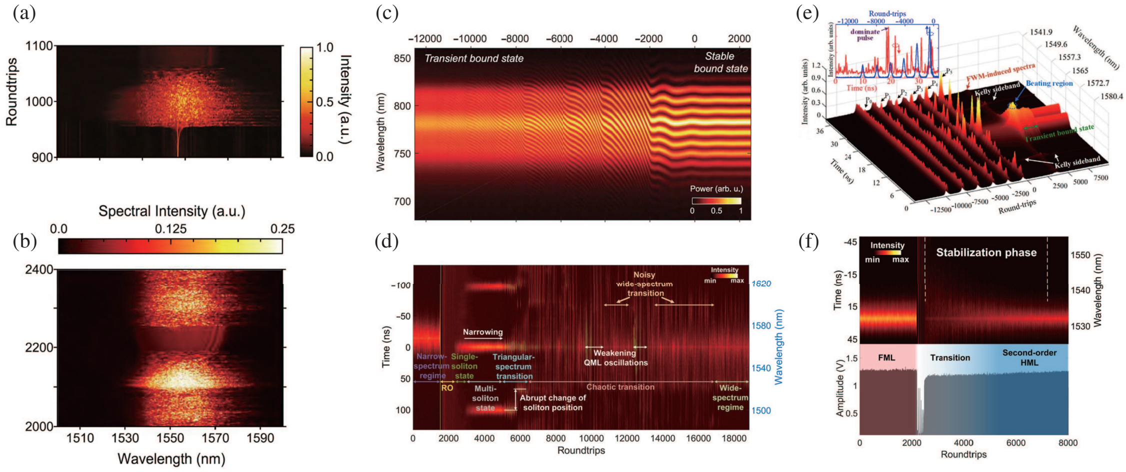

Figure 19 (Color online) Ultrafast nonlinear dynamics inside MLFLs observation using the TS-DFT. (a) Transition from the CW state to a stable FML regime; (b) soliton explosions. Reprinted with permission from [97] @Copyright 2019 Springer Nature. (c) Formation of a soliton molecule [98] @Copyright 2017 AAAS. (d) Transition dynamics from a narrow-spectrum FML regime to a wide-spectrum FML regime [92] @Copyright 2020 Springer Nature. (e) Characterizing the buildup process of a soliton molecule [99] @Copyright 2019 American Physical Society. (f) Transition dynamics from the FML regime to the second-order HML regime based on an intelligent MLFL [100] @Copyright 2019 IEEE.

essential to MLFLs and some studies have already appended pump power to the feedback control [63]. By intelligent pump power control, the stability of the FML regime can be improved by reducing the multi-pulsing instabilities and the HML regimes can be readily acquired by automatically increasing the pump power. Furthermore, the maximum pulse peak power can be obtained with the minimum pump power (by reducing the CW emissions and multi-pulsing instabilities) thereby promoting the energy efficiency of pump power. The fundamental repetition rate is another important feature of a pulse train. Owing to the inherent noises (i.e., the thermal noise and the shot noise) and environmental disturbances, the fundamental repetition rate is not fixed thereby causing the timing jitter of pulses [13]. However, with various piezoelectric (PZT) components including PZT-mounted mirrors, PZT-wound fiber, or PZT-attached fiber sections, we can vary the cavity length of the laser in a small range [95] which means that the fundamental repetition rate can be dynamically tuned in a small range as well [13]. By intelligent control on the cavity length via devices like PZT components and electro-optic modulators, the fundamental repetition rate can be rather stable and the time jitter of pulses can be significantly reduced [96]. Although some studies demonstrated the fundamental repetition rate stabilization using EPCs [73], altering the cavity length is a more direct method in controlling the fundamental repetition rate. In the current stage of AML techniques, researchers focus more on how to search the pulsation regimes automatically rather than the quality of the pulses. The next stage of AML techniques, as we see, is to acquire entire control on the laser output (both in temporal and spectral domains). Then, according to some application scenarios, the laser automatically operates under some specific pulsation regimes with specific temporal and spectral characteristics by intelligent control.

AML techniques have successfully addressed the difficulty of initial mode-locking and the detachments recovery in the traditional NPR-based MLFLs. Therefore, AML techniques can be applied in traditional NPR-based MLFLs to help them perform better in various applications of MLFLs [1–12]. Apart from bringing performance improvement for traditional NPR-based MLFLs, the emergence of AML techniques spawns some unique applications. Recently, ultrafast nonlinear dynamics inside MLFLs observation using the TS-DFT is a hot research topic as shown in Figure 19 [97–100]. The TS-DFT based real-time optical spectrum analysis provides immense possibilities for comprehension of ultrafast physical phenomena, including soliton explosions [97, 101], the mode-locking build-up process [97, 102], sophisticated soliton dynamics [30, 103] and the build-up process of soliton molecules [98, 99]. Now, with AML techniques, the transition dynamics between two arbitrary regimes can be readily observed via electronic polarization control after the two objective regimes are targeted by AML techniques. This is a new perspective looking into the internal mechanism of MLFLs supported by AML techniques, which is very hard for traditional MLFLs. Based on a home-made intelligent MLFL [66], we have demonstrated the regime transition dynamics among the CW state, the FML regime, the QS regime and the HML regimes [100] and the transition dynamics from the narrow-spectrum FML regime to the wide-spectrum FML regime [92]. However, more ultrafast transition dynamics inside MLFLs are still waiting to be discovered. For instance, the establishment of soliton molecules is experimentally demonstrated but transition dynamics involving bound-soliton states is still undiscovered. We believe that the process of unveiling the internal mechanism of MLFLs will be accelerated with new experimental insights provided by AML techniques.

6 Conclusion

Throughout the entire development of AML techniques, in the algorithmic perspective, AML techniques start from the straightforward but inefficient traversal algorithm and then evolve into the various optimization algorithms, machine learning and deep learning. The efficiency improvement of algorithms without doubt improves the efficiency of searching solutions corresponding to the desired pulsation regime in a tremendous, high-dimensional parametric space. On the other hand, in the hardware perspective, it is a good sign that real-time implementations become more and more popular recently in AML domain owing to the superior time-consuming performance. Apart for algorithm and implementation aspects, the objective function and discrimination criteria for the target regimes are essential to achieve the desired mode-locking regimes. AML techniques widen the applications of NPR-based MLFLs in both academic researches and industries for resolving the dilemma of NPR-based MLFLs. Combining with more controllable variables like pump power, PZT and various feedback signal, AML techniques will hold more control over the traditional MLFLs thereby contributing to more intelligent MLFLs. Furthermore, with TS-DFT, AML techniques support a new perspective to understand the internal mechanism of MLFLs by observing the ultrafast transition dynamics inside MLFLs, which is out the reach of traditional MLFLs.

Acknowledgements This work was supported by National Natural Science Foundation of China (Grant No. 61575122).

References

1 Udem T, Holzwarth R, Hansch T W. Optical frequency metrology. Nature, 2002, 416: 233–237
2 Jones D J, Diddams S A, Ranka J K, et al. Carrier-envelope phase control of femtosecond mode-locked lasers and direct optical frequency synthesis. Science, 2000, 288: 635–639
3 Reichert J, Holzwarth R, Udem T, et al. Measuring the frequency of light with mode-locked lasers. Opt Commun, 1999, 172: 59–68
4 Diddams S A, Jones D J, Ye J, et al. Direct link between microwave and optical frequencies with a 300 THz femtosecond laser comb. Phys Rev Lett, 2000, 84: 5102–5105
5 Bloom B J, Nicholson T L, Williams J R, et al. An optical lattice clock with accuracy and stability at the 10^{-18} level. Nature, 2014, 506: 71–75
6 Nemitz N, Ohkubo T, Takamoto M, et al. Frequency ratio of Yb and Sr clocks with 5×10^{-17} uncertainty at 150 seconds averaging time. Nat Photon, 2016, 10: 258–261
7 Khilo A, Spector S J, Grein M E, et al. Photonic ADC: overcoming the bottleneck of electronic jitter. Opt Express, 2012, 20: 4454–4469
8 Ghelfi P, Laghezza F, Scotti F, et al. A fully photonics-based coherent radar system. Nature, 2014, 507: 341–345
9 Lee J, Kim Y J, Lee K, et al. Time-of-flight measurement with femtosecond light pulses. Nat Photon, 2010, 4: 716–720
10 Coddington I, Swann W C, Nenadovic L, et al. Rapid and precise absolute distance measurements at long range. Nat Photon, 2009, 3: 351–356
11 Li C H, Benedick A J, Fendel P, et al. A laser frequency comb that enables radial velocity measurements with a precision of 1 cms^{-1}. Nature, 2008, 452: 610–612
12 Steinmetz T, Wilken T, Araujo-Hauck C, et al. Laser frequency combs for astronomical observations. Science, 2008, 321: 1335–1337
13 Kim J, Song Y. Ultralow-noise mode-locked fiber lasers and frequency combs: principles, status, and applications. Adv Opt Photon, 2016, 8: 465
14 Kuizenga D, Siegman A. FM and AM mode locking of the homogeneous laser–part I: theory. IEEE J Quantum Electron, 1970, 6: 694–708
15 Haus H A. Mode-locking of lasers. IEEE J Sel Top Quantum Electron, 2000, 6: 1173–1185

16 Zhang X, Hu H, Li W, et al. High-repetition-rate ultrashort pulsed fiber ring laser using hybrid mode locking. Appl Opt, 2016, 55: 7885–7891
17 Fu W, Wright L G, Sidorenko P, et al. Several new directions for ultrafast fiber lasers. Opt Express, 2018, 26: 9432–9463
18 Meng Y, Salhi M, Niang A, et al. Mode-locked Er:Yb-doped double-clad fiber laser with 75-nm tuning range. Opt Lett, 2015, 40: 1153–1156
19 Kang M S, Joly N Y, Russell P S J. Passive mode-locking of fiber ring laser at the 337th harmonic using gigahertz acoustic core resonances. Opt Lett, 2013, 38: 561–563
20 Amrani F, Haboucha A, Salhi M, et al. Passively mode-locked erbium-doped double-clad fiber laser operating at the 322nd harmonic. Opt Lett, 2009, 34: 2120–2122
21 Wang S, Wang Y, Feng G, et al. Harmonically mode-locked Yb: CALGO laser pumped by a single-mode 12 W laser diode. Opt Express, 2018, 26: 1521–1529
22 Zhang Z, Mou C, Yan Z, et al. Switchable dual-wavelength Q-switched and mode-locked fiber lasers using a large-angle tilted fiber grating. Opt Express, 2015, 23: 1353–1360
23 Chen Y, Jiang G, Chen S, et al. Mechanically exfoliated black phosphorus as a new saturable absorber for both Q-switching and Mode-locking laser operation. Opt Express, 2015, 23: 12823–12833
24 Kong L C, Xie G Q, Yuan P, et al. Passive Q-switching and Q-switched mode-locking operations of 2 m Tm: CLNGG laser with MoS 2 saturable absorber mirror. Photon Res, 2015, 3: 47–50
25 DeMaria A J, Stetser D A, Heynau H. Self mode-locking of lasers with saturable absorbers. Appl Phys Lett, 1966, 8: 174–176
26 Dudley J M, Genty G, Mussot A, et al. Rogue waves and analogies in optics and oceanography. Nat Rev Phys, 2019, 1: 675–689
27 Namiki S, Ippen E P, Haus H A, et al. Energy rate equations for mode-locked lasers. J Opt Soc Am B, 1997, 14: 2099–2111
28 Bale B G, Kieu K, Kutz J N, et al. Transition dynamics for multi-pulsing in mode-locked lasers. Opt Express, 2009, 17: 23137–23146
29 Li F, Wai P K A, Kutz J N. Geometrical description of the onset of multi-pulsing in mode-locked laser cavities. J Opt Soc Am B, 2010, 27: 2068–2077
30 Sun S Q, Lin Z X, Li W, et al. Time-stretch probing of ultra-fast soliton dynamics related to Q-switched instabilities in mode-locked fiber laser. Opt Express, 2018, 26: 20888–20901
31 Imai M, Terasawa Y, Ohtsuka Y. Polarization fluctuation characteristics of a highly birefringent fiber system under forced vibration. J Lightw Technol, 1988, 6: 720–727
32 Namihira Y, Wakabayashi H. Real-time measurements of polarization fluctuations in an optical fiber submarine cable in a deep-sea trial using electrooptic $LiNbO_3$ device. J Lightw Technol, 1989, 7: 1201–1206
33 Karlsson O, Brentel J, Andrekson P A. Long-term measurement of PMD and polarization drift in installed fibers. J Lightw Technol, 2000, 18: 941–951
34 Waddy D S, Lu P, Chen L, et al. Fast state of polarization changes in aerial fiber under different climatic conditions. IEEE Photon Technol Lett, 2001, 13: 1035–1037
35 Wuttke J, Krummrich P M, Rosch J. Polarization oscillations in aerial fiber caused by wind and power-line current. IEEE Photon Technol Lett, 2003, 15: 882–884
36 Willner A E, Nezam S M R M, Yan L, et al. Monitoring and control of polarization-related impairments in optical fiber systems. J Lightw Technol, 2004, 22: 106–125
37 Waddy D S, Chen L, Bao X. Polarization effects in aerial fibers. Opt Fiber Technol, 2005, 11: 1–19
38 Woodward S L, Nelson L E, Schneider C R, et al. Long-term observation of PMD and SOP on installed fiber routes. IEEE Photon Technol Lett, 2013, 26: 213–216
39 Hönninger C, Paschotta R, Morier-Genoud F, et al. Q-switching stability limits of continuous-wave passive mode locking. J Opt Soc Am B, 1999, 16: 46–56
40 Wang Y, Lin N, Gao W. Strain compensated robust semiconductor saturable absorber mirror for fiber lasers. Chin Opt Lett, 2019, 17: 071404
41 Krausz F, Brabec T, Spielmann C. Self-starting passive mode locking. Opt Lett, 1991, 16: 235–237
42 Tamura K, Haus H A, Ippen E P. Self-starting additive pulse mode-locked erbium fibre ring laser. Electron Lett, 1992, 28: 2226–2228
43 Matsas V J, Newson T P, Zervas M N. Self-starting passively mode-locked fibre ring laser exploiting nonlinear polarisation switching. Opt Commun, 1992, 92: 61–66
44 Nielsen C K, Ortaç B, Schreiber T, et al. Self-starting self-similar all-polarization maintaining Yb-doped fiber laser. Opt Express, 2005, 13: 9346–9351
45 Fermann M E, Andrejco M J, Stock Y, et al. Passive mode locking by using nonlinear polarization evolution in a polarization-maintaining erbium-doped fiber. Opt Lett, 1993, 18: 894–896
46 Sobon G, Sotor J, Abramski K M. All-polarization maintaining femtosecond Er-doped fiber laser mode-locked by graphene saturable absorber. Laser Phys Lett, 2012, 9: 581–586
47 Szczepanek J, Kardaś T M, Radzewicz C, et al. Ultrafast laser mode-locked using nonlinear polarization evolution in polarization maintaining fibers. Opt Lett, 2017, 42: 575–578
48 Turchinovich D, Liu X, Lægsgaard J. Monolithic all-PM femtosecond Yb-fiber laser stabilized with a narrow-band fiber Bragg grating and pulse-compressed in a hollow-core photonic crystal fiber. Opt Express, 2008, 16: 14004–14014

49 Liu X, Lægsgaard J, Turchinovich D. Highly-stable monolithic femtosecond Yb-fiber laser system based on photonic crystal fibers. Opt Express, 2010, 18: 15475–15483
50 Liu X, Lægsgaard J, Turchinovich D. Self-stabilization of a mode-locked femtosecond fiber laser using a photonic bandgap fiber. Opt Lett, 2010, 35: 913–915
51 Hellwig T, Walbaum T, Groß P, et al. Automated characterization and alignment of passively mode-locked fiber lasers based on nonlinear polarization rotation. Appl Phys B, 2010, 101: 565–570
52 Shen X, Li W, Yan M, et al. Electronic control of nonlinear-polarization-rotation mode locking in Yb-doped fiber lasers. Opt Lett, 2012, 37: 3426–3428
53 Radnatarov D, Khripunov S, Kobtsev S, et al. Automatic electronic-controlled mode locking self-start in fiber lasers with non-linear polarization evolution. Opt Express, 2013, 21: 20626–20631
54 Li S, Xu J, Chen G, et al. An automatic mode-locked system for passively mode-locked fiber laser. In: Proceedings of International Conference on Optical Instruments and Technology (OIT), Beijing, 2013. 9043
55 Olivier M, Gagnon M D, Piché M. Automated mode locking in nonlinear polarization rotation fiber lasers by detection of a discontinuous jump in the polarization state. Opt Express, 2015, 23: 6738–6746
56 Shen X, Hao Q, Zeng H. Self-tuning mode-locked fiber lasers based on prior collection of polarization settings. IEEE Photon Technol Lett, 2017, 29: 1719–1722
57 Pu G, Yi L, Zhang L, et al. Programmable and fast-switchable passively harmonic mode-locking fiber laser. In: Proceedings of Optical Fiber Communications Conference and Exposition (OFC), San Diego, 2018. W2A.9
58 Wu H H, Huang P H, Teng Y H, et al. Automatic generation of noise-like or mode-locked pulses in an Ytterbium-doped fiber laser by using two-photon-induced current for feedback. IEEE Photon J, 2018, 10: 1–8
59 Fu X, Kutz J N. High-energy mode-locked fiber lasers using multiple transmission filters and a genetic algorithm. Opt Express, 2013, 21: 6526–6537
60 Andral U, Fodil R S, Amrani F, et al. Fiber laser mode locked through an evolutionary algorithm. Optica, 2015, 2: 275–278
61 Andral U, Buguet J, Fodil R S, et al. Toward an autosetting mode-locked fiber laser cavity. J Opt Soc Am B, 2016, 33: 825–833
62 Woodward R I, Kelleher E J R. Towards 'smart lasers': self-optimisation of an ultrafast pulse source using a genetic algorithm. Sci Rep, 2016, 6: 37616
63 Woodward R I, Kelleher E J R. Genetic algorithm-based control of birefringent filtering for self-tuning, self-pulsing fiber lasers. Opt Lett, 2017, 42: 2952–2955
64 Winters D G, Kirchner M S, Backus S J, et al. Electronic initiation and optimization of nonlinear polarization evolution mode-locking in a fiber laser. Opt Express, 2017, 25: 33216–33225
65 Ryser M, Bacher C, Latt C, et al. Self-optimizing additive pulse mode-locked fiber laser: wavelength tuning and selective operation in continuous-wave or mode-locked regime. Fiber Lasers XV: Technol Syst, 2018, 10512: 1
66 Pu G, Yi L, Zhang L, et al. Intelligent programmable mode-locked fiber laser with a human-like algorithm. Optica, 2019, 6: 362–369
67 Pu G, Yi L, Zhang L, et al. Genetic algorithm-based fast real-time automatic mode-locked fiber laser. IEEE Photon Technol Lett, 2019, 32: 7–10
68 Brunton S L, Fu X, Kutz J N. Extremum-seeking control of a mode-locked laser. IEEE J Quantum Electron, 2013, 49: 852–861
69 Fu X, Brunton S L, Kutz J N. Classification of birefringence in mode-locked fiber lasers using machine learning and sparse representation. Opt Express, 2014, 22: 8585–8597
70 Brunton S L, Fu X, Kutz J N. Self-tuning fiber lasers. IEEE J Sel Top Quantum Electron, 2014, 20: 464–471
71 Kutz J N, Brunton S L. Intelligent systems for stabilizing mode-locked lasers and frequency combs: machine learning and equation-free control paradigms for self-tuning optics. Nanophotonics, 2015, 4: 459–471
72 Baumeister T, Brunton S L, Kutz J N. Deep learning and model predictive control for self-tuning mode-locked lasers. J Opt Soc Am B, 2018, 35: 617–626
73 Shen X, He B, Zhao J, et al. Repetition rate stabilization of an erbium-doped all-fiber laser via opto-mechanical control of the intracavity group velocity. Appl Phys Lett, 2015, 106: 031117
74 Horowitz M, Barad Y, Silberberg Y. Noiselike pulses witha broadband spectrum generated from an erbium-dopedfiber laser. Opt Lett, 1997, 22: 799–801
75 Zhao L M, Tang D Y, Wu J, et al. Noise-like pulse in a gain-guided soliton fiber laser. Opt Express, 2007, 15: 2145–2150
76 An Y, Shen D, Zhao W, et al. Characteristics of pulse evolution in mode-locked thulium-doped fiber laser. Opt Commun, 2012, 285: 1949–1953
77 Holland J H. Genetic algorithms. Scient Am, 1992, 267: 66–73
78 Özgören K, Ilday F Ö. All-fiber all-normal dispersion laser with a fiber-based Lyot filter. Opt Lett, 2010, 35: 1296–1298
79 Fedotov Y S, Kobtsev S M, Arif R N, et al. Spectrum-, pulsewidth-, and wavelength-switchable all-fiber mode-locked Yb laser with fiber based birefringent filter. Opt Express, 2012, 20: 17797–17805
80 Zhang Z X, Xu Z W, Zhang L. Tunable and switchable dual-wavelength dissipative soliton generation in an all-normal-dispersion Yb-doped fiber laser with birefringence fiber filter. Opt Express, 2012, 20: 26736–26742
81 Devore J L. Probability and Statistics for Engineering and the Sciences. Singapore: Cengage Learning, 2011
82 You X H, Zhang C, Tan X S, et al. AI for 5G: research directions and paradigms. Sci China Inf Sci, 2019, 62: 021301

83 Chen S T, Jian Z Q, Huang Y H, et al. Autonomous driving: cognitive construction and situation understanding. Sci China Inf Sci, 2019, 62: 081101

84 Habimana O, Li Y H, Li R X, et al. Sentiment analysis using deep learning approaches: an overview. Sci China Inf Sci, 2020, 63: 111102

85 Duda R, Hart P, Storck D. Pattern Classification. New York: Wiley, 2001

86 Bishop C M. Pattern Recognition and Machine Learning. New York: Springer, 2006

87 Murphy K. Machine Learning: A Probabilistic Perspective. Cambridge: MIT Press, 2012

88 Goodfellow I, Bengio Y, Courville A. Deep Learning. Cambridge: MIT Press, 2016

89 García C E, Prett D M, Morari M. Model predictive control: theory and practice-a survey. Automatica, 1989, 25: 335–348

90 Bhushan A S, Coppinger F, Jalali B. Time-stretched analogue-to-digital conversion. Electron Lett, 1998, 34: 839–841

91 Mahjoubfar A, Churkin D V, Barland S, et al. Time stretch and its applications. Nat Photon, 2017, 11: 341–351

92 Pu G, Yi L, Zhang L, et al. Intelligent control of mode-locked femtosecond pulses by time-stretch-assisted real-time spectral analysis. Light Sci Appl, 2020, 9: 13

93 Stratmann M, Pagel T, Mitschke F. Experimental observation of temporal soliton molecules. Phys Rev Lett, 2005, 95: 143902

94 Li L, Huang H, Su L, et al. Various soliton molecules in fiber systems. Appl Opt, 2019, 58: 2745–2753

95 Briles T C, Yost D C, Cingöz A, et al. Simple piezoelectric-actuated mirror with 180 kHz servo bandwidth. Opt Express, 2010, 18: 9739–9746

96 Hudson D D, Holman K W, Jones R J, et al. Mode-locked fiber laser frequency-controlled with an intracavity electro-optic modulator. Opt Lett, 2005, 30: 2948–2950

97 Lapre C, Billet C, Meng F, et al. Real-time characterization of spectral instabilities in a mode-locked fibre laser exhibiting soliton-similariton dynamics. Sci Rep, 2019, 9: 1–12

98 Herink G, Kurtz F, Jalali B, et al. Real-time spectral interferometry probes the internal dynamics of femtosecond soliton molecules. Science, 2017, 356: 50–54

99 Liu X, Yao X, Cui Y. Real-time observation of the buildup of soliton molecules. Phys Rev Lett, 2018, 121: 023905

100 Pu G, Yi L, Zhang L, et al. Real-time observation of the regime transition dynamics of mode-locked fiber lasers. IEEE Photon Technol Lett, 2019, 31: 1545–1548

101 Runge A F J, Broderick N G R, Erkintalo M. Observation of soliton explosions in a passively mode-locked fiber laser. Optica, 2015, 2: 36–39

102 Herink G, Jalali B, Ropers C, et al. Resolving the build-up of femtosecond mode-locking with single-shot spectroscopy at 90 MHz frame rate. Nat Photon, 2016, 10: 321–326

103 Ryczkowski P, Närhi M, Billet C, et al. Real-time full-field characterization of transient dissipative soliton dynamics in a mode-locked laser. Nat Photon, 2018, 12: 221–227